Science of the Total Environment 672 (2019) 212–226

Contents lists available at ScienceDirect

Science of the Total Environment

journal homepage: www.elsevier.com/locate/scitotenv

High time-resolved measurements of water-soluble sulfate, nitrate and ammonium in $PM_{2.5}$ and their precursor gases over the Eastern Mediterranean

Ersin Tutsak, Mustafa Koçak *

Institute of Marine Sciences, Middle East Technical University, P.O. Box 28, 33731 Erdemli-Mersin, Turkey

HIGHLIGHTS

- Comparison of online and offline measurements of sulfate, ammonium, nitrate in $PM_{2.5}$
- The temporal and diurnal variability of sulfate, ammonium, nitrate in $PM_{2.5}$ and their precursor gases
- The impact of air flow on measurements of sulfate, ammonium, nitrate in $PM_{2.5}$ and their precursor gases

GRAPHICAL ABSTRACT

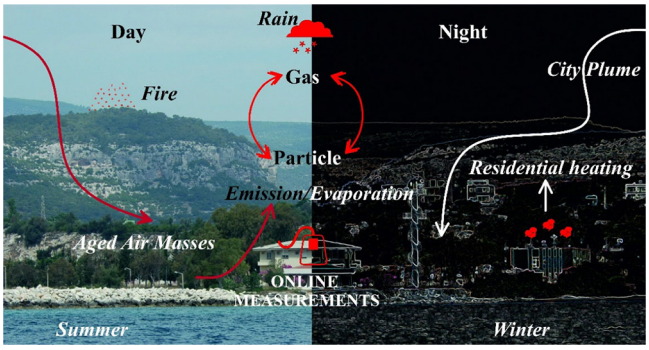

ARTICLE INFO

Article history:
Received 21 December 2018
Received in revised form 28 March 2019
Accepted 29 March 2019
Available online 01 April 2019

Editor: Jianmin Chen

Keywords:
Water-soluble SO_4^{2-}
NO_3^-
NH_4^+
Precursor gases
High time-resolved measurements
Eastern Mediterranean

ABSTRACT

High time-resolved measurements of aerosol SO_4^{2-}, NO_3^-, NH_4^+ and their precursor gases HNO_3, SO_2, NH_3 between 27 and 02 January/February and 19–01 August/September 2015 were carried out by applying AIM-IC at a rural site located on the coast of the Eastern Mediterranean, Erdemli, Turkey. The comparison between online and offline techniques revealed better correlation coefficients for SO_4^{2-} and NH_4^+ ($r > 0.90$) than that of NO_3^- (0.63). Mean concentrations of water-soluble species were found in decreasing order SO_4^{2-} (2814 ng m^{-3}) > NH_4^+ (1371 ng m^{-3}) > NO_3^- (495 ng m^{-3}). NH_3 (3390 ng m^{-3}) concentration was more than enough to neutralize SO_2 (879 ng m^{-3}) and HNO_3 (346 ng m^{-3}). The gas-to-particle conversion ratios (>0.3) implied that SO_4^{2-}, NO_3^- and NH_4^+ were mainly influenced by non-local sources. SO_4^{2-}, NO_3^-, NH_4^+, HNO_3, SO_2 exhibited remarkable decrease (leastways 40%) in the atmosphere over the Eastern Mediterranean throughout fifteen years. In winter, day time NH_3 concentrations illustrated significant relationship with temperature (positive) and humidity (negative), implying evaporation of dew or emission from plant stoma. Whereas, diurnal cycle of SO_4^{2-} and SO_2 was considerably influenced by populated City of Mersin in winter. During summer, HNO_3 and SO_2 ($r = 0.74$) demonstrated similar diurnal cycle, suggesting a common source for these precursor gases whilst NH_3 was considerably affected by biomass burning emissions. Variability of all species was governed by local or nearly mesoscale transport in winter possibly due to frequent rain events. In summer, air flow from Eastern Mediterranean denoted aged air masses (GPC > 0.65) containing rather uniform concentrations of SO_4^{2-} (~65 nmol m^{-3}) and NH_4^+

* Corresponding author.
E-mail address: mkocak@ims.metu.edu.tr (M. Koçak).

https://doi.org/10.1016/j.scitotenv.2019.03.451

(~140 nmol m^{-3}). The highest NH_3 along with the greatest % K_{BB} contribution to $PM_{2.5}$ mass was observed under the influence of Northerly airflow, exhibiting significance of biomass burning emissions as a source of NH_3 in summer.

1. Introduction

Aerosols consist of complex mixtures of soluble and insoluble particles and they play an essential role in various geophysical and geochemical processes such as altering the earth's climate directly by scattering and absorbing incoming solar radiation (Haywood and Shine, 1997), influencing the concentration and size distribution of cloud droplets, the distribution of rainfall and their radiative properties (Levin et al., 2005; Huang et al., 2006; Rosenfeld et al., 2008), acting as reaction surfaces in the atmosphere (Arimoto, 2001; Usher et al., 2003; Krueger et al., 2004), supplying macro and micro nutrients to the surface of the world oceans (Mahowald et al., 2005; Jickells et al., 2005; Paytan et al., 2009; Jordi et al., 2012) and impacting health (Salma et al., 2002; Hauck et al., 2004).

Conventionally, aerosol water-soluble ion composition is determined by offline analytical methods. First, atmospheric particles are collected on filters drawing air through a filter by means of a vacuum pump and then the determination of water-soluble ions in the aerosol is achieved by using ion chromatography after extraction. During such sampling or sample storage, chemical and physical changes may occur (Schaap et al., 2004). Therefore, offline techniques may lead to positive and negative artefacts during sampling and storage (Lipfert, 1994; Tsai and Perng, 1998; Hering and Cass, 1999; Pakkanen et al., 1999; Schaap et al., 2002; Schaap et al., 2004; Wieprecht et al., 2004; Keck and Wittmaack, 2005; Chow et al., 2008; Vecchi et al., 2009; Cheng et al., 2012). Offline sampling errors result from gas absorption by sampling material, gas-particle/particle-particle interactions, evaporation of collected aerosol species from filters, and meteorological conditions (such as temperature and humidity). Glass-fiber, quartz and cellulose acetate filters have been found to adsorb gaseous SO_2 and HNO_3 (Appel et al., 1984; Savoie et al., 1992). Acidic gases may also adsorb onto pre-existing alkaline particles such as sea salt and mineral dust. Such errors lead to positive bias. Nitrate volatilization may occur owing to (i) thermal decomposition, particularly when ambient temperature exceeds 20 °C and (ii) chemical reactions between NH_4NO_3 and H_2SO_4 and HCl (Appel et al., 1980; Appel and Tokiwa, 1981). Hering and Cass (1999) have reported about 30% loss of nitrate from Teflon filters and this volatilization has been attributed to either (i) scavenging of nitric acid and ammonia in the sampler inlet or (ii) heating the filter substrate. Schaap et al. (2004) have demonstrated that Teflon filters were more prone to evaporation losses than those of quartz filters.

In order to minimize sampling errors and improve temporal resolution for better comprehension of the atmospheric chemistry and physics of the aerosols, ion chromatography based high time-resolved measurements has been developed. Particle-Into-Liquid-Sampler coupled to ion chromatography (PILS-IC) was developed in the beginning of 2000 (Weber et al., 2001). On one hand, PILS-IC is capable of carrying out rapid, automated online measurements of ionic composition in $PM_{2.5}$ on the other hand, it is incapable of detecting precursor gases. Gas/Particle Ion Chromatography (GPIC, Ullah et al., 2006) has been utilized to determine ionic composition of $PM_{2.5}$ and precursor gases. This instrument is capable of measuring water-soluble ions and precursor gases such as chloride, nitrate, sulfate, ammonium, hydrochloric acid, nitric acid, sulfuric acid and ammonia. However, GPIC is not able to detect cations such as sodium, potassium, magnesium and calcium. Furthermore, gas and particle measurements cannot be carried out simultaneously, rather they must be staggered by 20 min. Monitor for AeRosols and Gases (MARGA, Applikon Analytical BV) has dual ion chromatography and it is capable of measuring water-soluble anions and cations (Ten Brink et al., 2007). Similar to MARGA, Ambient Ion Monitor – Ion Chromatography (AIM-IC) is an instrument capable of carrying out continuous, hourly simultaneous measurements of water-soluble ions in $PM_{2.5}$ and their precursor gases with a high accuracy and precision (Markovic et al., 2012).

There are few near real time measurements of aerosol SO_4^{2-}, NO_3^-, NH_4^+ and their precursor gases (HNO_3, SO_2, NH_3) in the Western Mediterranean (Di Gilio et al., 2015; Malaguti et al., 2015), however, based on our knowledge, there is no such studies in the Eastern Mediterranean. Thus, the current study presents for the first time high time-resolved sulfate, ammonium and nitrate in $PM_{2.5}$ and their precursor gases concentrations in winter and summer as well as gas-to-particle conversions in the atmosphere over the Eastern Mediterranean. This study aims to (i) compare online and offline results for SO_4^{2-}, NO_3^- and NH_4^+ (ii) explore decreases in SO_4^{2-}, NO_3^-, NH_4^+, HNO_3, SO_2, and NH_3 over the Eastern Mediterranean during last decade, (iii) investigate temporal and diurnal variability for winter and summer and (iv) assess the influence of the transport of air masses on SO_4^{2-}, NO_3^-, NH_4^+ and their precursor gases.

2. Material and method

2.1. Sampling site description

High time-resolved measurements of SO_4^{2-}, NO_3^-, NH_4^+, HNO_3, SO_2, and NH_3 were carried out at a rural site located on the coast of the Eastern Mediterranean, Erdemli, Turkey (36.57°N, 34.26°E). The site is surrounded by cultivated land and greenhouses, while the city of Mersin with a population of 800.000, with soda, chromium, and fertilizer producing industries and a thermic power plant on its periphery, is located 45 km to the east of the study area (for more details see Kubilay and Saydam, 1995; Koçak et al., 2012).

2.2. Ambient Ion Monitor Ion Chromatography (AIM-IC) measurements

Ambient **I**on **M**onitor **I**on **C**hromatography (AIM-IC) consists of two major components: (i) the sampling unit for the simultaneous collecting of aerosols in $PM_{2.5}$ and their precursor gases (AIM 9000D, URG Corp., Chapel Hill, NC) and (ii) the sample analysis unit, ion chromatography (ICS-5000, Thermo-Dionex) for the determination of anionic and cationic ions in the collected aqueous solution.

The online sample collection is carried out by drawing ambient air at 3 L min^{-1} through a pre-impaction (cyclone) assembly which intercepts the atmospheric particles that are bigger than 2.5 μm equivalent aerodynamic diameter. Therefore, only the atmospheric particles smaller than 2.5 μm are directed into the parallel-plate wet denuder. The parallel-plate wet denuder consists of two cellulose membranes (one per plate) that are continuously supplied with 5 mM of ultrapure hydrogen peroxide (H_2O_2) solution at 10 mL hr^{-1}. As the ambient air passes between the plates, soluble precursor gases are separated from the atmospheric particles by diffusion and dissolution into the denuder solution. The resultant solution from the denuder having dissolved gases is splinted into two 5 mL syringes for the detection of anionic and cationic species in the liquid. The air free of precursor gases, then flows into the particle supersaturation chamber, comprising of (i) a steam generator (ii) mixing/condensation chamber and (iii) a cyclone.

In the supersaturation chamber, the particles are activated by steam in order to initiate hygroscopic growth in the mixing/condensation chamber. The cyclone removes large and heavily solvated particles from the bulk air flow. The resultant solution from the supersaturation chamber is splinted into two 5 mL syringes for the determination of anionic and cationic species in the liquid. Before reaching the diaphragm pump, the remaining humidified air passes through Vigreux to eliminate water from the flowing air. After the sampling, the solutions are automatically injected into the ion chromatography instrument.

High time-resolved measurements of water-soluble anionic/cationic species in $PM_{2.5}$ and precursor gases were carried out under identical conditions by using an ICS-5000 ion chromatography instrument. Water-soluble anions (SO_4^{2-}, NO_3^-) and gases (HNO_3 and SO_2) were determined by applying AS11-HC separation column, KOH (gradient from 18 to 59 mM) eluent and AERS-500 (4 mm) suppressor whereas water-soluble cations (NH_4^+) and precursor gas (NH_3) were detected electrochemically by using a CS12-A separation column, MSA (20 mM) eluent and CSRS-300 (4 mm) suppressor (Product Manual for Dionex IonPac AS11-HC-4 m, IonPac CS12A Manual). The anions and cation calibrations (Dionex six cation standard-II for cation and seven anion standard-II for anion) were performed at the beginning and at the end of each campaign (winter: from January 27 to February 3, summer: between August 19 and September 2). The limit of detection for SO_4^{2-}, NO_3^-, NH_4^+, HNO_3, SO_2, and NH_3 was better than 0.1 μg m^{-3}.

Near real time hourly measurements were performed using the AIM-IC during the winter period between January 27 and February 3 and the summer period between August 19 and September 2, 2015. From time to time, the measurements were temporarily interrupted for technical reasons during the online sampling campaigns. 127 and 307 measurements were attained in the winter period and the summer period, respectively. In order to compare results from online measurements, offline $PM_{2.5}$ samples were simultaneously collected during the sampling campaign. Offline $PM_{2.5}$ samples were collected on 47 mm Teflon filters (0.8 μm pore size) by using a Thermo-Scientific 2000i Partisol Air Sampler with a flow rate of 16.7 L min^{-1}. Offline aerosol sampling campaign commenced on 21 August 2015 and ended on 02 September 2015. The samples were stored in a deep-freezer (−20 °C) directly after collection until analysis. In order to determine concentrations of major water-soluble ions in the aerosol, one quarter of the filter was extracted for 45 min in 20 mL of ultra-pure water (18.2 Ω) by mechanic shaker. The extraction was treated with about 100 μL chloroform to prevent biological activity (Bardouki et al., 2003; Koçak et al., 2007). The water-soluble ions concentrations were measured by using the ICS-5000 ion chromatography instrument as described above. The detection limit for water-soluble SO_4^{2-}, NO_3^- and NH_4^+ was <0.001 μg m^{-3} while the blank contributions were smaller than 1%.

2.3. Local meteorology, cloud cover and air mass back trajectory categorization

Meteorological parameters (for statistical summary see Table S1) play a vital role in the variability of aerosols and their precursor gases as well as gas-to-particle conversions. Winter was the wettest season and hence rain was particularly intensive from 27th to 31st of the January 2015, which is likely to lead to the removal of aerosols and their precursor gases from the atmosphere by wet deposition. In contrast, there was no rain in the summer during sampling. Surface air temperature was at least 2 times higher in summer (28.2 °C) compared to winter (11.5 °C). The sea surface pressure was higher in winter (1016.4 hPa) than in summer (1007.9 hPa), implying comparatively stable weather conditions in winter. During the winter the average relative humidity was 75.6%, whilst it was 59.6% during summer. Wind direction and speed exhibited a great difference between winter and summer (see Fig. S1). The wind speed was higher in summer (1.6 m s^{-1}) than that observed in winter (1.2 m s^{-1}). During winter most of the winds originated from the north, explaining 82.3% of the wind direction whilst the highest wind speeds were associated with Easterlies (2.0 m s^{-1}) and East-North-Easterlies (1.6 m s^{-1}). It is worth mentioning there was no southerly winds during the winter campaign. During summer, northerly and southerly winds had almost equal importance, arising during 45.7% and 41.4% of the period, respectively. In general, the northerly winds were more sluggish (varying from 0.7 m s^{-1} to 1.6 m s^{-1}) than those observed for southerly winds (ranging between 1.6 m s^{-1} and 2.6 m s^{-1}). Hourly total cloud fractions were produced averaging values of grids over the region between 34°E-35°E and 36°N-37°N from MERRA-2 (M2T1NXRAD).

Since there was no statistical difference between air masses back trajectories in winter (implying local or nearly mesoscale transport rather than long range transport, for more details see Section 3.7), the categorization of air masses for winter will not be discussed in this section. Hourly two-day backward trajectories arriving at Erdemli for the summer campaign were calculated using the HYSPLIT Model driven by Global Data Assimilation System (GDAS) data (HybridSingle Particle Langrangian Integrated Trajectory; Draxler, 1999; Stein et al., 2015). The planetary boundary layer (PBL) heights were computed with HYSPLIT every 3 h employing the Kantha-Clayson vertical turbulence scheme. Air mass back trajectories reaching the height of 200 m were applied considering the lowest planetary boundary height that was observed in summer (see Fig. 6).

Hourly air masses back trajectories for summer were categorized into four groups (see Fig. S2, Koçak et al., 2009 and references therein). Starting from northwest, this airflow (Northwest: NW) emerged from Greece; then, air masses passed through the Aegean Sea and the west region of Turkey before arriving at the sampling site, explaining 3.2% of the trajectories. The second (North: N) airflow originated from north Turkey, clarifying 58.2% of the air masses. The third category (Southwest-short: SWS) exhibited sluggish airflow originating from the Mediterranean Sea, then sweeping the south coastline of Turkey before reaching the site, accounting for 32.7% of the trajectories. The fourth group (Mediterranean: MED) indicated airflow coming from the center of the Mediterranean Sea, explaining 5.8% of air masses back trajectories.

3. Results and discussion

3.1. Comparison of online and offline measurements

In order to evaluate and compare the results from online and offline techniques, 24 hourly data obtained from AIM-IC were utilized to calculate the arithmetic means to be comparable with the collection time of the offline samples. The percentage difference (% D, see Eq. (S1)) for each sample between the online and offline values (see Table S2) were calculated as suggested by Malaguti et al. (2015).

Comparison of online and offline measurements has been made by several authors (Drewnick et al., 2003; Nie et al., 2010; Xue et al., 2011; Makkonen et al., 2012; Malaguti et al., 2015). These studies have shown that results obtained from the two techniques for sulfate and ammonium were comparable exhibiting good correlation coefficients. In contrast, comparisons of nitrate have indicated poor correlation coefficients with a remarkable difference in concentrations attained from online and offline measurements (Nie et al., 2010; Malaguti et al., 2015). Fig. 1 shows plots of online concentrations against offline for sulfate, ammonium and nitrate achieved from online and offline measurements. The residual correlation coefficients (R^2) for sulfate (0.99) and ammonium (0.91) were considerably better than that achieved for nitrate (0.63). The slope of the regression lines for sulfate and ammonium were higher than unity, being 1.33 and 1.08, respectively, whilst the slope for nitrate was 0.4. The slope of the regressions suggests a positive bias for sulfate and ammonium and a negative bias for nitrate. Negative biases have been reported for offline nitrate as well as ammonium sampling compared to online measurements

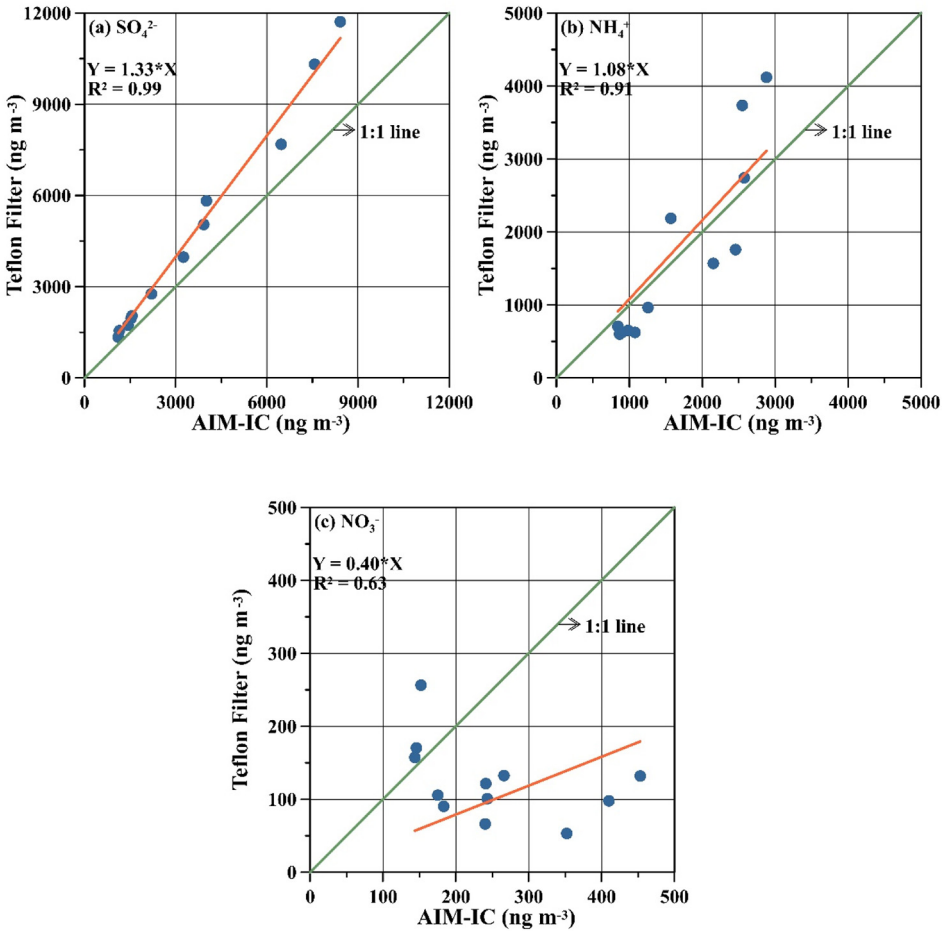

Fig. 1. Scatter plots of sulfate (**a**), ammonium (**b**) and nitrate (**c**) obtained from AIM-IC and Teflon Filters.

(Chow et al., 2008; Nie et al., 2010; Makkonen et al., 2014; Malaguti et al., 2015).

Sulfate concentrations from the online technique for all measurements were lower than those obtained from the offline technique, having a % difference varying between −16 and −31% (see Table S2). Nonetheless, the % difference between online and offline measurements for ammonium and nitrate was relatively complex compared to sulfate. At the beginning of the experiment the % difference was positive then it was negative until the end of the experiment. Fig. 2 shows the relationship between enhanced non sea salt sulfate (en-nssSO_4^{2-} = offline-nssSO_4^{2-} - online-nssSO_4^{2-}) and offline-Na^+ (indicator of sea salt) in neq m^{-3}. nssSO_4^{2-} concentration was calculated as $nssSO_4^{-2} = SO_4^{-2} - Na^+ * 0.252$,where the coefficient of 0.252 is the usual sulfate to sodium mass ratio in bulk seawater (Millero and Sohn, 1992; during the study the sea salt contribution to sulfate in $PM_{2.5}$ was not >2%). A statistically significant residual correlation coefficient ($R^2 = 0.85$) was found between en-nssSO_4^{2-} and Na^+. Therefore, the difference between offline and online techniques for sulfate might be ascribed to the enhancement of sulfate because of either (i) the reaction between acidic H_2SO_4 and preexisting sea salt particles or (ii) oxidation of SO_2 on the surface of preexisting sea salt particles.

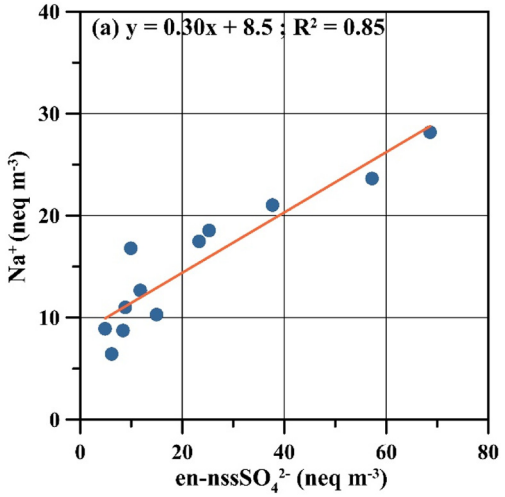

Fig. 2. Scatter plot of enhanced non sea salt sulfate (en-nssSO_4^{2-} = offline-nssSO_4^{2-} - online-nssSO_4^{2-}) and offline-Na^+.

It has been stated that the gas-particle partitioning may promote dissociation of ammonium nitrate (Vecchi et al., 2009). The partial correlations between temperature/relative humidity/particle-to-gas ratio and ammonium/nitrate are given in Table S3. The percent difference for ammonium and nitrate was mainly influenced by partitioning between gas and aerosol phase. % D increased with decreasing ammonium in particle phase for ammonium, whilst % D decreased with increasing nitric acid likely owing to adsorption of nitric acid on alkaline particles. % D for ammonium and nitrate also exhibited a statistically important relationship with temperature, suggesting evaporation from the Teflon Filters during off-line sampling. On the other hand, the % D of nitrate denoted increase under dry conditions, promoting nitrate evaporation from the filter substrate with increasing temperature.

Table 1
Statistical summary for SO_4^{2-}; NH_4^+, NO_3^- in $PM_{2.5}$ (ng m^{-3}) and their precursor gases along with gas-to-particle (molar) ratios.

Species	Arithmetic mean	Standard deviation	Minimum	Maximum	Median	Geometric mean	Skewness
SO_4^{2-}	2814	2620	120	10,233	1755	1701	1.11
NH_4^+	1371	1016	39	4796	1168	958	0.90
NO_3^-	495	568	64	3891	260	320	2.59
SO_2	879	1329	101	10,334	499	574	4.63
NH_3	3330	4896	72	54,927	1394	1834	4.66
HNO_3	346	168	55	1440	302	320	3.03
$SO_4^{2-}/SO_4^{2-} + SO_2$	0.62	0.27	0.02	0.95	0.68	0.53	
$NH_4^+/NH_4^+ + NH_3$	0.38	0.24	0.01	0.86	0.35	0.28	
$NO_3^-/NO_3^- + HNO_3$	0.50	0.17	0.09	0.90	0.46	0.47	

3.2. General characteristics of data set

The statistical summary for SO_4^{2-}, NH_4^+, NO_3^- (in $PM_{2.5}$), SO_2, NH_3 and HNO_3 including arithmetic mean, standard deviations, median, minimum and maximum, and geometric mean for the Erdemli site are presented in Table 1. The minimum and maximum concentrations as well as the standard deviations exhibit large variability in both period. Such high variability has been reported for semi-continuous SO_4^{2-}, NH_4^+, NO_3^-, SO_2, NH_3 and HNO_3 measurements (Godri et al., 2009; Du et al., 2010; Shi et al., 2014; Tian et al., 2017). The large variability may be ascribed to (i) local meteorological parameters (such as temperature, relative humidity, rain, solar irradiance and wind direction), (ii) type of source, (iii) emission strength of source, (iv) proximity to source, (v) history of air masses and (vi) chemical transformation and removal of species throughout middle and long range of transport.

In general, the arithmetic mean, median and geometric mean values for SO_4^{2-}, NH_4^+, NO_3^-, SO_2, NH_3 and HNO_3 showed considerable difference between arithmetic mean concentrations and geometric means/medians, the former being higher than those of later whereas geometric means and medians were comparable. The skewness also indicates that the species were not normally distributed. The non-parametric Kolmogorov-Smirnov statistical test exhibited that the above mentioned species were lognormally distributed within the 90% confidence level (see Fig. S3).

Of the water-soluble ions in $PM_{2.5}$, sulfate and ammonium were the dominant species. Arithmetic mean sulfate and ammonium concentrations were 2814 ng m^{-3} and 1371 ng m^{-3}, ranging between 120 and 10,233 ng m^{-3} and 39–4796 ng m^{-3}, respectively. Aerosol nitrate ranged between 64 ng m^{-3} and 3891 ng m^{-3} with an arithmetic mean of 495 ng m^{-3}. Among the precursor gases, ammonia exhibited the highest concentration with a value of 3330 ng m^{-3}, fluctuating between 72 ng m^{-3} and 54,927 ng m^{-3}. Sulfur dioxide and nitric acid concentrations varied from 101 to 10,334 ng m^{-3} to 55–1440 ng m^{-3}, with mean concentrations of 879 ng m^{-3} and 346 ng m^{-3}, respectively. Taking into account precursor gases concentrations, it is clear that alkaline ammonia (g) concentration was more than enough to neutralize acidic gases. The arithmetic mean of gas-to-particle ratios for sulfate, ammonium and nitrate were respectively found to be 0.62 ± 0.25, 0.38 ± 0.24 and 0.50 ± 0.17. The gas-to-particle ratios for sulfate, ammonium and nitrate fluctuated from 0.01 to 0.97. It has been argued that ratios < 0.3 indicates local sources (Di Gilio et al., 2015 and references therein). In contrast, ratios larger than 0.3 denotes aged air masses with higher values implying older air masses and/or larger travelling distances (Di Gilio et al., 2015 and references therein). Thus, regarding arithmetic means of gas-to-particle conversion ratios for sulfate, ammonium and nitrate, it might be suggested that the concentrations of these species were mainly influenced by non-local sources.

3.3. Comparison of the current real time study with data from literature

In order to define spatial and long term difference in the concentrations of sulfate, ammonium, nitrate, sulfur dioxide, ammonia and nitric acid two types of data from literature will be used namely, (i) online and (ii) offline (for more information see Section S3.3).

The concentrations of sulfate, ammonium, nitrate, sulfur dioxide, ammonia and nitric acid obtained from online measurements along with offline measurements carried out in the Eastern Mediterranean are presented in Table 2. Generally, the highest concentrations of sulfate, ammonium, nitrate and ammonia concentrations were found over China (Du et al., 2011; Gao et al., 2011, 2016). Aerosol sulfate (from 14,000 to 40,000 ng m^{-3}), ammonium (from 9000 to 22,000 ng m^{-3}), nitrate (from 15,000 to 33,000 ng m^{-3}), sulfur dioxide (Beijin: 6650 ng m^{-3}) and ammonia (Beijing: 24540 ng m^{-3}), concentrations over China were an order of magnitude higher than those of observed for Erdemli. The sampling sites at China were heavily influenced by anthropogenic emissions such as traffic, fossil fuel combustion, man induced biomass burning and construction (Du et al., 2011; Gao et al., 2011, 2016). Aerosol sulfate, ammonium, nitrate and nitric acid concentrations over Italy (Bari and Trisaia) were comparable to the values obtained at Erdemli. In contrast, the mean ammonia (3330 ng m^{-3})

Table 2
Arithmetic mean concentrations of sulfate, ammonium, nitrate, sulfur dioxide, ammonia and nitric acid (ng m^{-3}) obtained from online for different sites of the world and offline for the Eastern Mediterranean.

Site	SO_4^{2-}	NH_4^+	NO_3^-	SO_2	NH_3	HNO_3	Reference	Character
Online								
Erdemli, Turkey	2810	1370	490	880	3330	350	This study	Rural
Bari, Italy	2430	2800	400	2040	1570	320	Di Gilio et al. [2015]	Urban
Trisaia, Italy	18,700	1030	520	–	–	–	Malaguti et al. [2015]	Rural
Shanghai, China	28,710	19,310	32,930	–	–	–	Du et al. [2011]	Urban
Jinan, China	38,330	21,260	15,770	–	–	–	Gao et al. [2011]	Urban
Beijing, China	14,800	8900	15,180	6650	24,540	–	Gao et al. [2016]	Urban
Singapore	4410	1760	1290	21,770	2470	3000	Behera et al. [2013]	Urban
Seoul, Korea	5800	3910	13,780	3580	4800	8710	Shon et al. [2012]	Urban
Bakersfield, USA	530	460	800	1830	13,690	360	Markovic et al. [2014]	Urban
Offline								
Finokalia, Greece	3940	1010	1630	4000	310	1860	Kouvarakis et al. [2001, 2002]	Natural
Patras, Greece				–	3200	2600	Danalatos and Glavas [1999]	Urban
Jerusalem, Israel	12,290	–	–	17,790	–	–	Luria et al. [1996]	Rural

concentration at Erdemli was about two times higher compared to that of Bari (1570 ng m^{-3}), Italy. However, the detected sulfur dioxide (880 ng m^{-3}) concentration for Erdemli was half of that observed at Bari (2040 ng m^{-3}). This distinct difference might be attributed to the influences at the sampling sites, the former being surrounded by cultivated soil and the latter being urban and influenced by the comparatively high emissions from heavy traffic. The highest nitric acid concentrations were observed at Seoul (8710 ng m^{-3}) and at Singapore (3000 ng m^{-3}) where concentrations were at least nine times higher than those detected at Erdemli (350 ng m^{-3}). These high values might be ascribed to the night time production of nitric acid due to NO_x emissions from heavy traffic close to the vicinity. Although ammonia concentrations at the Erdemli site are influenced by cultivated soil, the value observed at Bakersfield (13,690 ng m^{-3}) was 4 times higher than that of Erdemli (3330 ng m^{-3}) since Bakersfield is located in a huge agricultural region.

Taking into account this study and historic off-line measurements, there was a decreasing trend in the concentrations of sulfate, nitrate and their precursor gases in the Eastern Mediterranean atmosphere. Nitrate, sulfur dioxide and nitric acid were respectively found to show 3.3, 4.6 and 5.3 times decreases compared to results reported by Kouvarakis et al. (2001, 2002). Similar decreases in the concentrations of sulfur dioxide and nitrate have respectively been reported for the Mediterranean (Lelieveld et al., 2002) and the Black Sea (Koçak et al., 2016). The decrease for sulfate was 1.4 relative to Finokalia, however, sulfate concentration was 4.4 times less than that of Jerusalem. Ammonium and ammonia concentrations at Erdemli were larger than those for Finokalia because the Erdemli site is surrounded by an agricultural area. Table 3 shows the recent (January 2014–April 2015) and historical (March 2001–April 2002) offline $nssSO_4^{2-}$, NO_3^- and NH_4^+ concentrations at Erdemli. During the thirteen years, the percentanges of decreases for $nssSO_4^{2-}$, NO_3^- and NH_4^+ at the Erdemli sampling site in offline measurements were 55%, 40% and 50%, respectively. These results also support the negative trend in the concentrations of sulfate, nitrate and ammonium.

3.4. Temporal variations of sulfate, ammonium, nitrate in $PM_{2.5}$ and their precursor gases

A number of studies have demonstrated that sulfate, ammonium and nitrate in $PM_{2.5}$ as well as their precursor gases may exhibit large hourly variability in their concentrations (Nie et al., 2010; Makkonen et al., 2012; Markovic et al., 2014; Malaguti et al., 2015). As stated above, such a high variability may arise from (i) local meteorological parameter (such as temperature, relative humidity, rain, solar irradiance and wind direction), (ii) type of source, (iii) emission strength of source, (iv) proximity to source, (v) history of air masses and (vi) chemical transformation and removal of species throughout middle and long range transport.

Fig. 3 shows the hourly variations in the concentrations of SO_4^{2-}, NH_4^+, NO_3^-, SO_2, NH_3 and HNO_3 together with corresponding gas-to-particle conversion ratios and local meteorological parameters from 27 January to 03 February 2015 and from 19 August to 01 September 2015 at the Erdemli station. It is clear that all species exhibit a considerable variability, with the concentrations of the individual species fluctuating up to an order of magnitude from one hour to another during the study period. Aerosol sulfate and ammonium in $PM_{2.5}$ showed their lowest concentrations in winter particularly during rain events since these particles were efficiently scavenged by wet precipitation. For instance, a rain event started at around 23.00 pm on 29th of January 2015 and lasted 8 h. Just one hour before the rain started, aerosol sulfate and ammonium (nitrate) concentrations were 913 ng m^{-3} and 1035 ng m^{-3} (3890 ng m^{-3}), respectively. Within a few hours of consequential rain, aerosol sulfate and ammonium (nitrate) exhibited an order of magnitude decrease in their concentrations reaching down to 100 ng m^{-3} and 50 ng m^{-3} (280 ng m^{-3}) respectively. In addition to removal of particles by rain, lower gas-to-particle conversion may also contribute to observed lower concentrations of these aerosol species due to inferior solar radiation in winter. Even though, aerosol nitrate concentration was influenced by wet scavenging in winter, it exhibited lower concentrations in summer. This might be attributed to (i) evaporation of nitrate due to either elevated temperatures (reaching up to 40 °C during the day), (ii) reaction between H_2SO_4 and NH_4NO_3 (Appel et al., 1980; Appel and Tokiwa, 1981) or (iii) emission from vehicles and stagnant air masses in winter (Di Gilio et al., 2015). High concentrations of SO_2 were observed in winter compared to summer. In winter, elevated concentrations of SO_2 might resulted from (i) residential heating, (ii) enhanced power generation by using high sulfur containing coal combustion, (iii) inferior gas-to-particle conversion, (iv) lower boundary layer height which prevents dilution of sulfur dioxide. In contrast, gas NH_3 exhibited lower concentrations in winter than during summer. The soil moisture and temperature have been identified as one of the controlling factors for NH_3 emissions (Roelle and Aneja, 2002). On the one hand, it has been demonstrated that NH_3 flux increases with increasing soil temperature, although, Roelle and Aneja (2002) suggested that rainwater may fill pores of the soil and prevent NH_3 diffusion from the soil to the air. Prevailing meteorological conditions such as rain and temperature may lead to lower NH_3 concentrations in winter. HNO_3 also demonstrated large variability whereas, observed concentrations in winter and summer were comparable. SO_2 and NH_3 concentrations were also influenced by rain events however, the decrease in their concentrations were less remarkable compared to aerosols. During the aforementioned rain events, SO_2 and NH_3 concentrations were respectively found to decrease from 2100 ng m^{-3} to 600 and from 500 ng m^{-3} to 240 ng m^{-3}. Gas-to-particle conversion ratios for sulfate, ammonium and nitrate remarkably changed from one hour to another. Except for nitrate, the conversion ratios for summer were higher than that calculated for winter.

To illustrate the influence of air mass transport on the temporal variation of the measured concentrations, an event characterized from August 25th to 27th will be discussed. Before the event, on 24th August, air masses originated from the west and southwest sectors (Fig. 4a) reaching the Erdemli site at 200 m, with a daily mean NH_3 concentration of 1088 ng m^{-3}. The next day, on 25th August at 07:00 am (local time), the airflow shifted to a northerly direction (Fig. 4b). During the following hours, the NH_3 concentration began to rise steadily and reached 2180 ng m^{-3} at 00:00 am on 26th August. Hourly 2-day back trajectories from 26th to 27th August showed that the transport pathway extended over the northeastern Black Sea and Russian and remained prevailing until end of the event (Fig. 4c, d). NH_3 continued to increase and reached its highest value at 01:00 am on 27th August, attaining 54,910 ng m^{-3}. The second maximum in NH_3 concentrations was also observed with a value of 26,180 ng m^{-3} at 13:00 pm on 27th August. The arithmetic mean of NH_3 values for this event was 8330 ng m^{-3}. The gas-to-particle conversion ratio for ammonium decreased to 0.10 during the event whilst it was around 0.65 just before the event. Since atmospheric NH_3 mostly has a life of 1 day (Seinfeld and Pandis, 1998), emission sources might be within the range of one-day transport. Meanwhile, NH_4^+ ($nnsSO_4^{2-}$) was found to decrease by about 50% (65%), reaching the mean concentration of 990 (1920) ng m^{-3} during the event. On the other hand, SO_2 increased substantially during the event with a time lag of one day to NH_3, reaching 960 ng m^{-3}. In

Table 3
Recent and historical offline $nssSO_4^{2-}$, NO_3^- and NH_4^+ concentrations at Erdemli (ng m^{-3}).

Species	Erdemli[a] 2014–2015	Erdemli[b] Historical	% Decrease
$nssSO_4^{2-}$	1880	4150	55
NO_3^-	1110	1860	40
NH_4^+	420	850	50

[a] Unpublished data.
[b] Koçak et al. (2007).

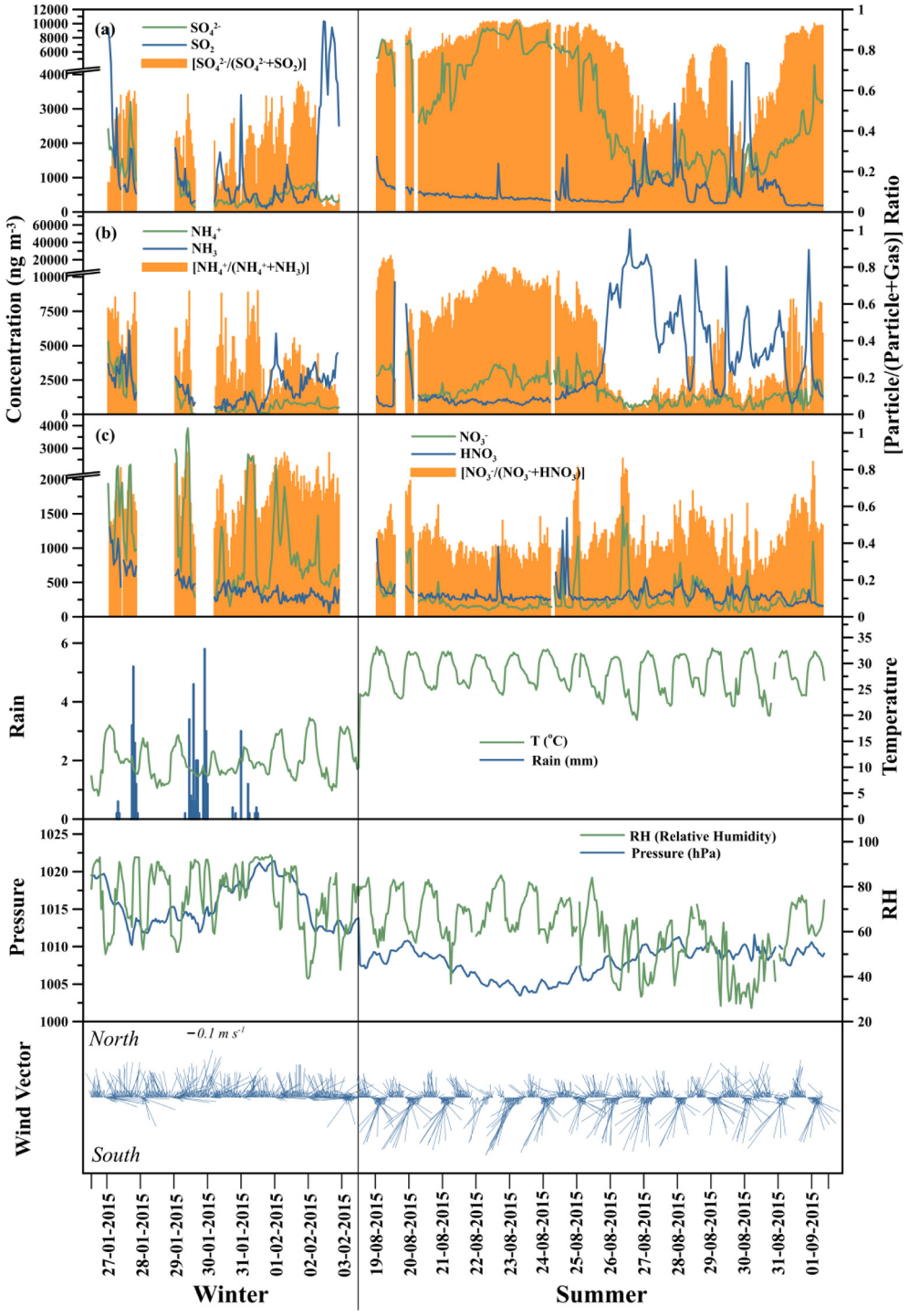

Fig. 3. Hourly variability of sulfate, ammonium and nitrate in $PM_{2.5}$ and their precursor gases along with gas-to-particle conversion ratios (molar) and meteorological parameters from to 27 January–03 February 2015 to 19 August–01 September 2015 at Erdemli station.

other words, SO_2 hourly variations did not show a similar pattern with NH_3. MODIS-Terra (Moderate Resolution Imaging Spectrometer) AOD satellite images indicated a slight decrease in optical thickness over site from 24th to 27th August. Daily concentrations from Teflon filters also supported the same amount of decrease in nnsSO_4^{2-} and NH_4^+. Moreover, the fraction of potassium associated with biomass burning (K_{BB}) and NH_3 correlated well ($r = 0.80$) during summer time indicating their origin from similar sources. Potassium has been used as an inorganic tracer of biomass burning (Ramadan et al., 2000; Ma et al., 2003; Liu et al., 2005; Lee et al., 2008) and K_{BB} can be calculated via using the formula ($K_{BB}^+ = K^+ - 0.036Na^+ - 0.12\,(Ca_{nss}^{2+} - Ca_{BB}^{2+})$ suggested by Pio et al. (2008). High levels of NH_3 are also emitted through biomass burning (Hegg et al., 1988; Crutzen and Andreae, 1990). Taking into account air mass histories and active fire spots in Fig. 4, this sharp increase in NH_3 may be attributed to either man or natural induced biomass burning.

3.5. Correlation between sulfate, ammonium, nitrate in $PM_{2.5}$ and their precursor gases

Correlation between variables shows the degree to which they vary together. Strong correlation coefficients between two species may be

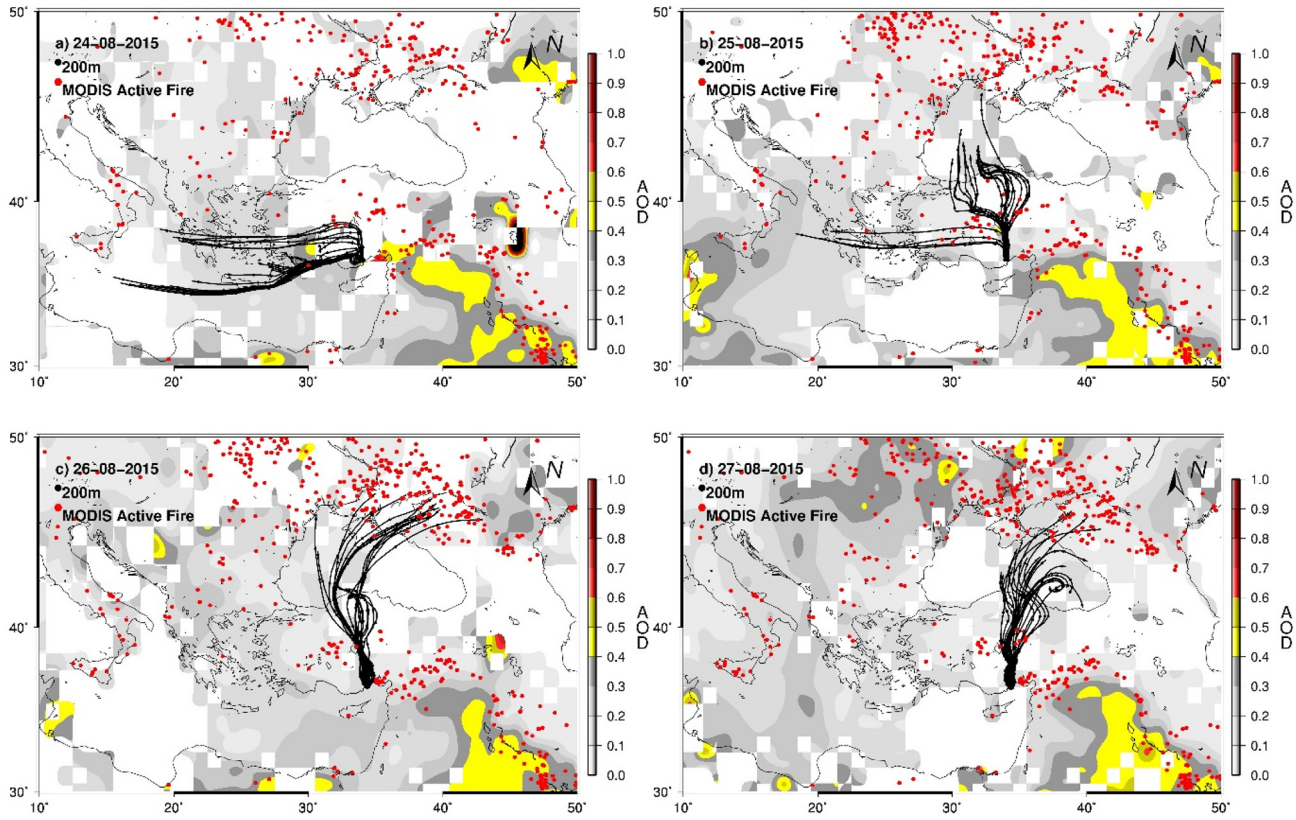

Fig. 4. Two-day back trajectories demonstrating the transport of air masses to Erdemli for every hour at 200 m and MODIS aerosol optical depth (AOD) and active fire (red) spots on 24 August 2015 (**a**), 25 August 2015 (**b**), 26 August 2015 (**c**), 27 August 2015 (**d**). (For interpretation of the references to colour in this figure legend, the reader is referred to the web version of this article.)

because of one or more of the following common processes: (a) similar sources (b) similar generation and/or removal mechanism and/or (c) similar transport patterns. The significance level of the correlation coefficient strictly depends on the number of samples. As a result, for populations with a high number of samples, even a small correlation coefficient can be statistically significant. Thus, five different terms will be used during the interpretation of correlation coefficients derived from the current datasets: (a) no correlation (r = 0), (b) weak correlation (r = 0–0.4), (c) moderate correlation (0.4–0.7) (d) strong correlation (0.7–1.0) and (d) perfect correlation ($r = 1.0$). Correlation coefficients between variables are illustrated in Table 4 [(a) winter and (b) summer].

Table 4
Correlation coefficient matrix of water-soluble ions in $PM_{2.5}$ and precursor gases along with meteorological parameters at Erdemli in winter (**a**) and summer (**b**).

a) Winter	SO_4^{2-}	NH_4^+	NO_3^-	SO_2	NH_3	HHO_3	T	RH	AP
SO_4^{2-}	1.00								
NH_4^+	0.90	1.00							
NO_3^-	*0.44*	0.70	1.00						
SO_2	0.15	0.11	−0.10	1.00					
NH_3	*0.49*	*0.47*	0.28	0.27	1.00				
HNO_3	0.70	0.74	0.36	−0.02	0.19	1.00			
T	0.33	0.28	0.21	−0.18	*0.47*	0.30	1.00		
RH	−0.36	−0.22	−0.04	−0.17	*−0.44*	−0.15	−0.73	1.00	
AP	−0.37	−0.31	−0.02	*−0.42*	−0.38	−0.21	0.01	*0.44*	1.00
b) Summer	SO_4^{2-}	NH_4^+	NO_3^-	SO_2	NH_3	HHO_3	T	RH	AP
SO_4^{2-}	1.00								
NH_4^+	0.84	1.00							
NO_3^-	−0.08	0.06	1.00						
SO_2	−0.24	−0.21	0.17	1.00					
NH_3	*−0.44*	*−0.41*	0.28	0.22	1.00				
HNO_3	0.09	0.12	0.24	*0.44*	0.14	1.00			
T	0.23	0.22	0.04	0.07	−0.13	0.01	1.00		
RH	*0.54*	*0.50*	−0.02	*−0.41*	−0.38	0.00	−0.34	1.00	
AP	−0.77	*−0.55*	0.30	0.32	0.36	0.03	0.01	*−0.46*	1.00

T: temperature. RH: relative humidity. AP: atmospheric pressure.

a) Winter

Ammonium showed strong correlation coefficients with sulfate and nitrate of 0.90 and 0.71, respectively. At the coastal Eastern Mediterranean, it has been shown that the ammonium levels were enough to neutralize acidic sulfate and nitrate during the winter (Koçak et al., 2007). The thermal stability of the NH_4NO_3 increases with decreasing temperature or from hot dry summer towards cold winter (Bennett, 1972). In order to clarify the forms of ammonium in the winter multi linear regression analysis (MLR) was applied. The results obtained were statistically significant with $p < 0.00001$. Estimated ammonium concentrations from MRL against measured concentrations of ammonium are illustrated in Fig. 5. The slope of the regression line was 1.00 with a correlation coefficient value of 0.96, implying acidic species sulfate and nitrate were completely neutralized by alkaline ammonium. Results from MRL also demonstrated that 60% of the ammonium presented in the form of $(NH_4)_2SO_4$ whilst 40% was in the form of NH_4NO_3 under the prevailing winter conditions. SO_4^{2-} (NO_3^-) and SO_2 (HNO_3) showed a weak correlation coefficient with a value of 0.15 (0.36), implying that sulfate (nitrate) primarily originated from non-local sources. HNO_3 exhibited strong correlations coefficients with sulfate and ammonium, of 0.70 and 0.74, respectively. It might be argued that these species either originated from the same source or had similar transport pattern. Gaseous ammonia exhibited moderate correlation coefficients with aerosol ammonium (0.47) and sulfate (0.49). This relationship suggested that the secondary ammonium and sulfate formation was partially influenced by locally emitted ammonia. Moreover, ammonia and temperature

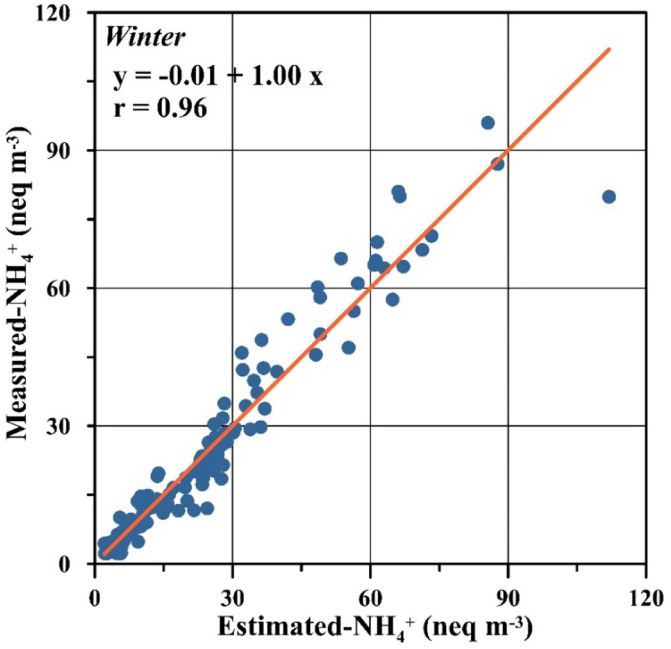

Fig. 5. Comparison of measured and estimated hourly concentrations from MRL for NH_4^+ in winter.

denoted a moderate correlation coefficient with a value of 0.47 and this might be attributed to (i) release of ammonium from leaf and vegetation surfaces, or (ii) evaporation of dew (Ellis et al., 2011; Wentworth et al., 2014, 2016). By comparison, ammonia showed moderate negative correlation coefficient with RH (−0.44) most likely due to enhanced formation of NH_4NO_3 under humid conditions (Chang et al., 1986).

b) Summer

As expected, there was a strong correlation coefficient (0.84) between ammonium and sulfate in summer. The slope of the regression line was 0.82 when sulfate was plotted against ammonium in neq m^{-3}. The value of 0.82 implies that ammonium levels were also enough to neutralize acidic sulfate in summer. These findings contradict with the previous results documented for the same site (Koçak et al., 2007). This discrepancy may be chiefly ascribed to the enhancement of sulfate particles throughout the off-line sampling campaigns (for more details see Section 3.1). Correspondingly, gaseous ammonia/sulfur dioxide and RH exhibited moderate negative and positive correlation coefficients with sulfate (−0.41 and 0.54) and ammonia (−0.41 and 0.50), suggesting an influence of RH on gas-to-particle conversions of ammonium and sulfate during more humid conditions in summer. There was a moderate correlation coefficient between SO_2 and HNO_3 (0.44), denoting that these gaseous species somewhat originated from similar source or air-mass. Sulfate and ammonium respectively indicated strong (−0.77) and moderate (−0.55) negative correlation coefficient with sea surface pressure. Elevated levels of sulfate and ammonium under the unsettled weather conditions might have resulted from either middle or long range transport since these particles have a relatively longer lifetime in summer (Koçak et al., 2007).

3.6. Diurnal variability

Typically, the concentrations of sulfate, ammonium, nitrate and their precursor gases demonstrate large diurnal variability (Gao et al., 2011; Shon et al., 2013; Hu et al., 2014; Makkonen et al., 2014; Markovic et al., 2014). Short-term changes in the concentrations of aforementioned species and gas-to-particle conversions can be very complex, arising from a combination of factors: (i) meteorological parameters such as temperature, solar influx, relative humidity, rain, wind speed/direction, sea surface pressure, cloud cover and boundary layer height, (ii) chemical reactions, (iii) source strength, (iv) type of source and (v) history of air masses (Kadowaki, 1986; Khoder, 2002; Wittig et al., 2004; Gao et al., 2011; Hu et al., 2014).

The arithmetic mean diurnal variability of sulfate, ammonium, nitrate and their precursor gases as well as the gas-to-particle conversions for winter and summer are illustrated in Fig. 6. Taking into account the diurnal variations for winter and summer, the following general observations may be made:

(a) Winter

SO_4^{2-} and SO_2 (see Fig. 6a) concentrations did not show dramatic changes from 00.00 to 02.00, demonstrating low values around 5 (480) and 16 nmol m^{-3} (1025 ng m^{-3}), respectively. These low concentrations may chiefly be attributed to removal of both species by wet deposition (see Fig. 6f) despite a shallow planetary boundary layer (~450 m, see Fig. 6e). From 02.00 to 03.00, SO_4^{2-} and SO_2 concentrations respectively increased 60 and 40% and reached the first peak at 04.00 with corresponding values of 10.1 (970) and 37.5 nmol m^{-3} (2402 ng m^{-3}), when rain events ceased between 02.00 and 05.00. After this peak, there was a sharp decrease in the concentrations of SO_4^{2-} and SO_2 until 10.00, reaching correspondingly 4.2 (403) and 14.8 nmol m^{-3} (948 ng m^{-3}), because of sequential rain events that occurred between 05.00 and 08.00. From 10.00 to 12.00, SO_4^{2-} and SO_2 exhibited a significant increase, attaining their highest concentrations with values of 11.7 (1124) and 42.7 nmol m^{-3} (2736 ng m^{-3}) when the airflow originated from the highly populated City of Mersin. Both species then demonstrated a gradual decline in their concentrations until 17.00 in the afternoon particularly under the influence of Easterly winds that may bring relatively less polluted air-masses originating from the sea. SO_4^{2-} showed more or less constant concentrations after sunset (from 17.00 to 23.00) however, SO_2 concentrations increased from 10 (641) to 34 nmol m^{-3} (2178 ng m^{-3}) between 17.00 and 23.00. The increment in SO_2 after sunset might be ascribed to (i) residential heating due to cold, (ii) decrease in PBL, (iii) change in airflow from Easterly (sea breeze) to Northerly (land breeze) and/or (iv) relatively a less efficient gas-to-particle conversion.

Ammonia exhibited a slight increase between 00.00 and 07.00 (sun rise about at 06.45), reaching 55.1 nmol m^{-3} (938 ng m^{-3}) with a 20% increase. From sun rise (07.00) to midday (12.00), there was a considerable increase in the concentration of ammonia, which reached a maximum at 12.00 with a value of 93.7 nmol m^{-3} (1596 ng m^{-3}). Ammonia concentration gradually decreased from 12.00 to 23.00, returning to the night time concentrations of around 50 nmol m^{-3} (852 ng m^{-3}). As can be seen from Fig. 6b and d, the diurnal trend of ammonia was coincident with the diurnal cycle of temperature and relative humidity. Correspondingly, the diurnal relationship of ammonia with temperature and RH were positive ($r = 0.88$) and negative ($r = -0.83$), suggesting a release of ammonia from dew as well as emissions from vegetation under hot and dry conditions or elevated formation of particle ammonium when the temperature is high and the relative humidity is low. Fig. 7a and b respectively exhibit the relationship of ammonia with temperature and RH for hourly measurements obtained during day and night time. During the day time, there was a significant correlation coefficient ($r = 0.76$) between ammonia concentration and temperature, however; this relationship was insignificant during night time. On the other hand, the correlation coefficients between ammonia concentration and relative humidity for day and night time ($r = -0.56$) and night ($r = -0.45$) were comparable, the former being slightly higher than that of later. Since ammonia respectively showed strong positive and moderate negative correlation coefficients with temperature and humidity, the day time increment might be ascribed to either

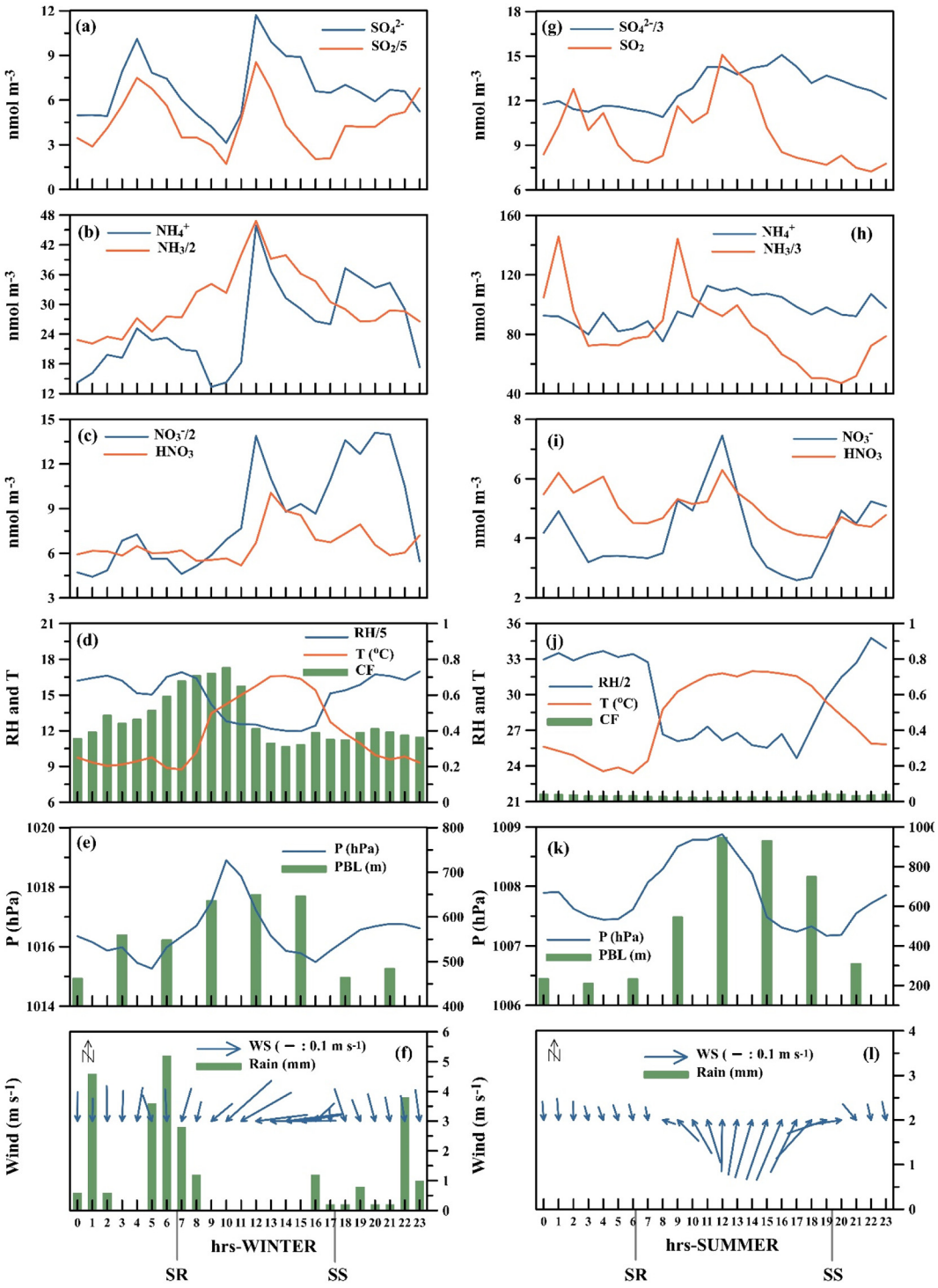

Fig. 6. Diurnal variability of sulfate, ammonium and nitrate in $PM_{2.5}$ and their precursor gases and meteorological parameters in winter and summer. SR and SS refer to Sun Rise and Sun Set, respectively.

evaporation of dew or emission from plant stoma. Whereas the night time decrease was more likely due to uptake of ammonia by plant and/or enhanced particle ammonium formation under low temperature (mean ~ 10 °C) and humid conditions.

The diurnal cycle of NH_4^+ was similar to that observed for NO_3^-. Both species exhibited low concentrations from 00.00 to 10.00. Within two hours, NH_4^+ and NO_3^- concentrations steeply increased and reached their first maximum at 12.00 with values of 46 (830) and 28 nmol m^{-3} (1736 ng m^{-3}), respectively. Afterwards, their concentrations dropped about 40% between 12.00 and 17.00, values respectively reaching down to 26.6 (453) and 17.3 nmol m^{-3} (1073 ng m^{-3}) when the site was affected by comparatively clean Easterly (sea breeze) winds. NH_4^+ as well as NO_3^- correspondingly showed a 40% and 60% rise in their concentrations peculiarly after sunset (17.00), illustrating a broader second peak compared to the first peak. The second peak appeared from 17.00 to 22.00 and might be connected with (i) decline in temperature and increase in RH, (ii) decrease in PBL and (iii) airflow from rather polluted air-masses originating from the North. Over the next two hours, the concentrations of NH_4^+ and NO_3^- exhibited a remarkable decrease, going down to 17.3 (290) and 10.7 nmol m^{-3} (663 ng m^{-3}) owing primarily

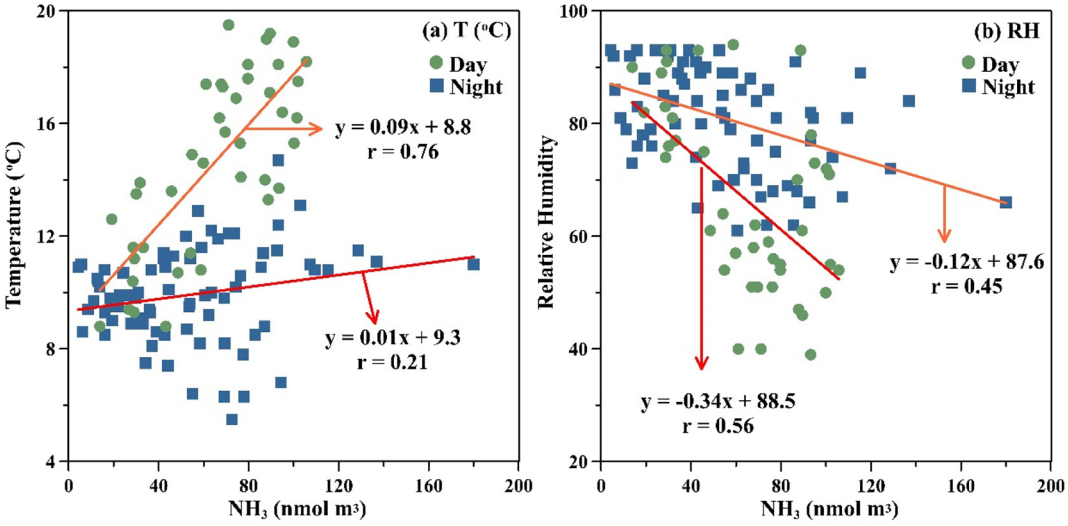

Fig. 7. The relationship of NH_3 with temperature (**a**) and relative humidity (**b**) in winter.

to efficient removal of these particles from the atmospheric compartment by wet deposition. HNO_3 exhibited a peak at 12.00, following the NH_4^+ and NO_3^- peaks at 11.00, which might be attributed to the dissociation of NH_4NO_3 owing to enhanced temperature and reduced relative humidity.

(b) Summer

From 00.00 to 08.00, sulfate and ammonium (Fig. 6g, h) did not exhibit a considerable change in their concentrations, being around 33 (3170) and 85 nmol m^{-3} (1533 ng m^{-3}), respectively. These low and constant values may chiefly be attributed to the lack of photochemical activities during the night and a sluggish northerly airflow associated with low sulfate and ammonium concentrations (see Section 3.7). Sulfate and ammonium concentrations increased about 30% and 45% respectively between 08.00 and 12.00 and they demonstrated a broad peak from 09.00 to 18.00. This might chiefly be attributed to enhanced gas-to-particle conversion in spite of the dilution effect owing to elevated PBL. From 00.00 to 01.00 SO_2 concentration (Fig. 6h) augmented 25% and reached the first peak at 02.00 with a value of 12.8 nmol m^{-3} (820 ng m^{-3}). After this peak, there was a decreasing tendency in the concentration of SO_2 until 07.00, reaching 7.8 nmol m^{-3} (500 ng m^{-3}). From 07.00 to 12.00, SO_2 demonstrated a remarkable increase, attaining its highest concentrations with a value of 15.1 nmol m^{-3} (967 ng m^{-3}). These two sharp peaks might be ascribed to northerly air flow relatively polluted with SO_2. Following that, SO_2 declined steadily until 19.00, when it reached a value of 7.5 nmol m^{-3} (480 ng m^{-3}). The decrement in SO_2 might be a result of relatively high gas-to-particle conversion and/or an increase in the PBL. SO_2 then showed more or less similar concentrations from 17.00 to 23.00. NH_3 (Fig. 6h) concentration reached the first peak at 01.00 with a value of 437.7 nmol m^{-3} (7454 ng m^{-3}). After this peak, there was a 50% decrease in the concentration of NH_3 until 03.00 when a value of 216.9 nmol m^{-3} (3694 ng m^{-3}) was recorded. From 03.00 to 08.00, NH_3 did not exhibit a remarkable change in its concentration (~230 nmol m^{-3} or 3917 ng m^{-3}). Then, NH_3 concentration increased sharply, denoting the second peak at 09.00 with a value of 433 nmol m^{-3} (7374 ng m^{-3}). This two maxima peaks in NH_3 possibly resulted from biomass burning events that affected the site (for more details see Section 3.7). Afterwards, NH_3 decreased from 10.00 to 20.00, reaching its lowest concentration with a value of 141.4 nmol m^{-3} (2408 ng m^{-3}). This dramatic decrease might be linked to either efficient gas-to-particle conversion or an increase in the PBL. NO_3^- (Fig. 6i) exhibited low concentrations from 00.00 to 08.00. Subsequently, NO_3^- concentration increased steeply and attained its maximum at 12.00 with a value of 7.5 nmol m^{-3} (465 ng m^{-3}). Within 2 h, its concentrations dropped by about 50% and continued to decrease until 18.00, reaching a value of 2.7 nmol m^{-3} (167 ng m^{-3}). The sudden decrease of NO_3^- might be attributed to thermal decomposition of NO_3^- with increasing temperature and/or an increase in the PBL. After sunset (from 19.00 to 23.00), NO_3^- showed a significant increase, going up to 5.1 nmol m^{-3} (316 ng m^{-3}). The diurnal cycle of HNO_3 was similar to that of observed for SO_2 ($r = 0.74$, $p < 0.01$), suggesting a common source for these precursor gases. HNO_3 illustrated rather large values from 00.00 to 04.00, ranging between 5.5 (347) and 6.2 nmol m^{-3} (391 ng m^{-3}). HNO_3 exhibited a second peak at 12.00 which was coincident with NO_3^- and SO_2 peaks. These HNO_3 peaks may arise from night time production of nitric acid (Brown et al., 2006) and rather polluted northerly air flow.

3.7. Influence of air flow on high time-resolved measurements of water-soluble ions in $PM_{2.5}$ and precursor gases

The Kruskal-Wallis (K—W, $p > 0.05$) test was applied to evaluate the impact of air masses back trajectories on the high time-resolved measurements of SO_4^{2-}, NH_4^+, NO_3^-, SO_2, NH_3, HNO_3. The results from the K—W test did not reveal any statistically significant difference between airflows in winter. This might be ascribed to frequent rain events (5 rainy days out of total 8 measurement days) during the winter campaign, implying local or nearly mesoscale transport rather than long range transport. Therefore, classification for winter was done according to local wind direction. Fig. 8 demonstrates the arithmetic means for sulfate, ammonium and nitrate and their precursor gases as well as gas-to-particle conversion ratios as a function of the local wind directions in winter and air mass back trajectory clusters in summer.

3.7.1. Winter

Except for the cases of SO_4^{2-} and NH_3, the K—W test did not reveal any statistically significant difference between local wind directions for NH_4^+, NO_3^-, SO_2 and HNO_3. The observed concentrations of NH_4^+, NO_3^-, SO_2 and HNO_3 might chiefly originated from local sources such as traffic, residential heating and Erdemli town situated at 7 km NE of the sampling site. The K—W test demonstrated that SO_4^{2-} concentration was remarkably higher when local airflow originated from the East, being at least 40% larger than during other wind directions. These relatively high values may be attributed to the pollution plume coming from the City of Mersin and industry areas located at the east of the sampling site and the absence of rain in Easterly airflow. Similarly, the K—W test

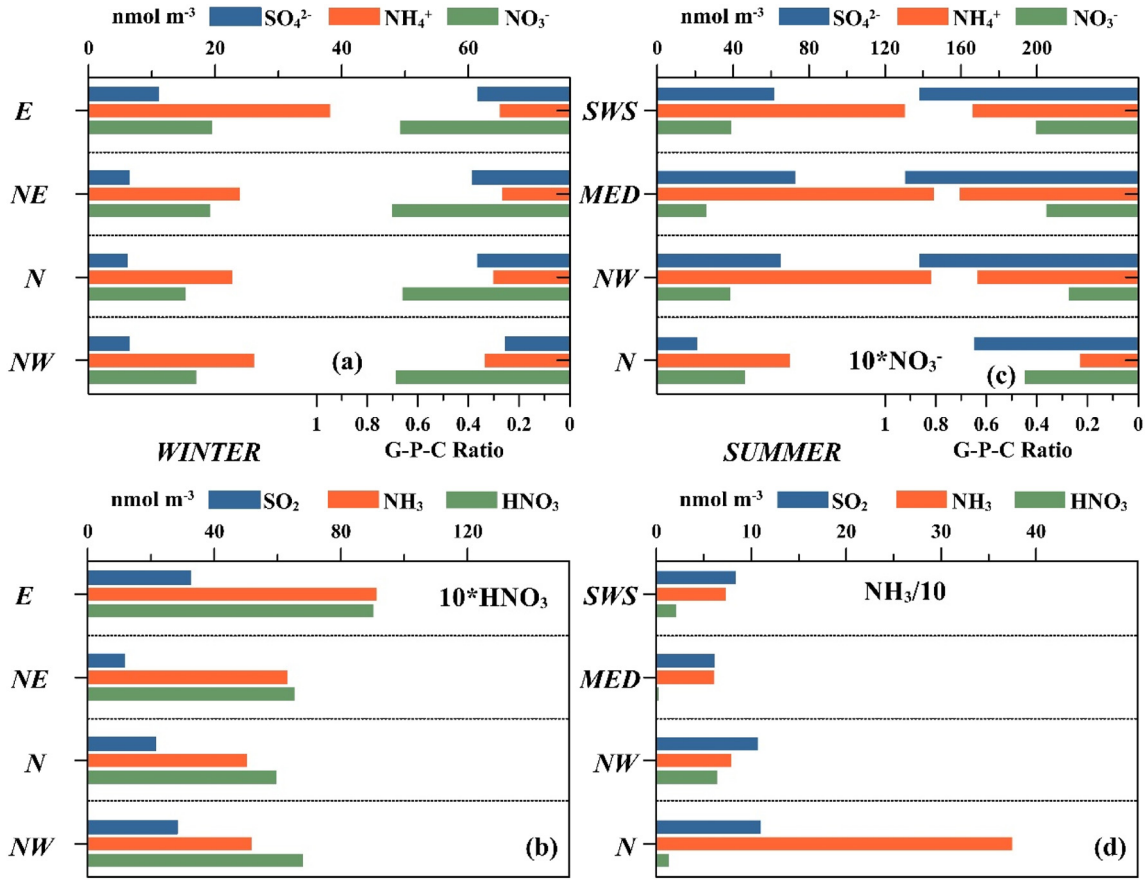

Fig. 8. Arithmetic means for sulfate, ammonium and nitrate and their precursor gases as well as gas-to-particle conversion (G-P-C) ratios as a function of the local wind directions in winter (**a**–**b**) and air mass back trajectory sectors in summer (**c**–**d**).

showed statistically significant differences between Easterly and NW, N as well as NE airflows. NH_3 for the E sector was at least 30% higher than values calculated for the remaining airflow directions. Additionally, the highest temperature and the lowest humidity at the sampling site was observed when airflow originated from East (for a statistical summary of meteorology see Table S4). Regarding these peculiarities, high ammonia in Easterly airflow might be ascribed to both evaporation of dew/emission from plant stoma (for more details see Section 3.6) and the influence of the City of Mersin as well as the fertilizer industry positioned to the East of the site. Gas-to-particle conversion ratios of SO_4^{2-}, NH_4^+ and NO_3^- for airflows were found to be similar, being around 0.3 and 0.70 for SO_4^{2-}/NH_4^+ and NO_3^-, respectively. Particularly low gas-to-particle conversion ratios of SO_4^{2-} and NH_4^+ support the idea that the observed concentrations of species were mainly influenced by local or nearly mesoscale transport rather than long range transport.

3.7.2. Summer

The K—W test did not show any difference between air masses for NO_3^-, HNO_3 and, SO_2. The lowest SO_4^{2-} (21.0 nmol m^{-3} or 2017 ng m^{-3}) and NH_4^+ (69.8 nmol m^{-3} or 1259 ng m^{-3}) concentrations were associated with airflow from the North, and were at least 2.9 and 1.9 times lower than those observed for the remaining airflows (K—W test, $p < 0.05$). Whereas, the K—W test did not show a statistically significant difference for SO_4^{2-} (~65 nmol m^{-3} or 6244 ng m^{-3}) and NH_4^+ (~140 nmol m^{-3} or 2525 ng m^{-3}) between SWS, MED and NW airflows with a comparatively high relative humidity (for statistical summary of meteorology see Table S4). It has been shown that transboundary transport of secondary aerosols actively takes place over Europe and Eurasia while the atmosphere over the Eastern Mediterranean acts as a reservoir under the prevailing summer conditions (Koçak et al., 2011). Fig. 9 presents SO_4^{2-} surface mass concentration for August 2015 from MERRA-2. A reanalysis image exhibited almost uniform distribution of SO_4^{2-} over the Eastern Mediterranean including the Aegean Sea, of around 55 nmol m^{-3} (5283 ng m^{-3}) which was surprisingly similar those of observed at Erdemli under the influence of SWS, MED and NW airflows. Furthermore gas-to-particle conversion ratios for these airflows were also comparable for SO_4^{2-} (~0.88) and NH_4^+ (~0.68), suggesting that the air masses arriving at the station from these directions were aged (Luria et al., 1996). The highest NH_3 concentration (6400 ng m^{-3} or 375 nmol m^{-3}) and the lowest gas-to-particle conversion ratio (0.16) were associated with northerly airflow, and correspondingly, their means were at least 4.7 times larger and 4.1 times smaller than those of remaining airflows. As aforementioned, biomass burning (see Section 3.4) can be an important source of NH_3 (Hegg et al., 1988; Crutzen and Andreae, 1990). Fig. 10 illustrates NH_3 concentrations along with % K_{BB} contributions to $PM_{2.5}$ mass for before (under the influence of SWS, MED and NW airflows), during (N airflow) and after (N airflow) biomass burning events. % K_{BB} contribution to $PM_{2.5}$ was 0.26 before biomass burning events then % K_{BB} contribution increased 4.5 times during biomass burning events, reaching up to 1.18%. After biomass burning ceased, the % K_{BB} contribution dropped to 0.30. The highest NH_3 concentration (8500 ng m^{-3} or 500 nmol m^{-3}) was associated with the largest % K_{BB} contribution to $PM_{2.5}$. Consequently, it might be argued that NH_3 values observed in northerly airflow were likely influenced by biomass burning emissions.

4. Summary and conclusion

The current study has yielded nearly real time datasets of water-soluble SO_4^{2-}, NH_4^+, NO_3^- (in $PM_{2.5}$), SO_2, NH_3 and HNO_3 during winter and summer at a coastal rural site on the Eastern Mediterranean. Based on results the following summary may be made:

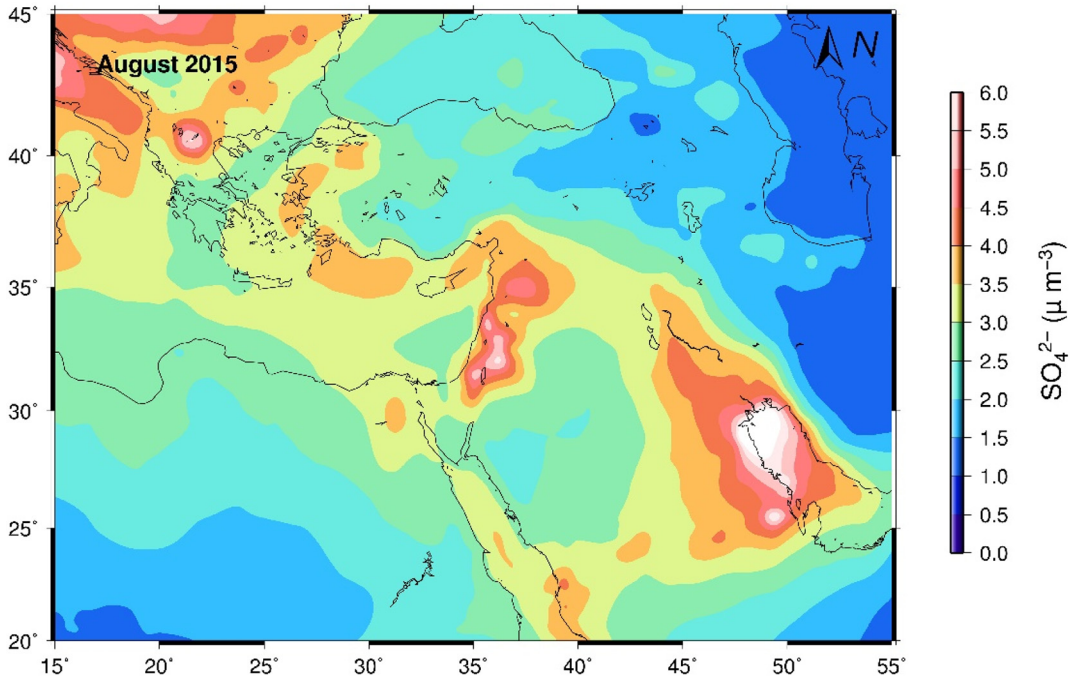

Fig. 9. SO_4^{2-} surface mass concertation for August 2015 from MERRA-2 (atmospheric reanalysis for the satellite era using the Goddard Earth Observing System Model).

SO_4^{2-} exhibited a positive bias for the offline technique since enhancement of SO_4^{2-} would occur on the surface of preexisting sea salt particles whereas the percent difference between online and offline techniques for NH_4^+ and NO_3^- was mainly influenced by partitioning between the gas and aerosol phase.

SO_4^{2-} (2814 ng m^{-3}) concentrations were about two and five times higher than those of NH_4^+ (1371 ng m^{-3}) and NO_3^- (495 ng m^{-3}). Precursor gases were dominated by NH_3 (3330 ng m^{-3}and the alkaline NH_3 concentration was more than enough to neutralize acidic gases (SO_2 = 879 ng m^{-3}, HNO_3 = 346 ng m^{-3}). Gas-to-particle conversion ratios for SO_4^{2-}, NH_4^+ and NO_3^- were higher than value of 0.3, implying that concentrations of these species were mainly influenced by non-local sources.

SO_4^{2-}, NH_4^+, NO_3^-, SO_2 and HNO_3 (except for NH_3) exhibited a remarkable decrease across the Eastern Mediterranean. The decrease in SO_2 and HNO_3 was at least 70% whilst the reduction in water-soluble nssSO_4^{2-}, NO_3^- and NH_4^+ was about 40% over the Eastern Mediterranean.

NO_3^- denoted lower concentrations in summer due to evaporation of nitrate whilst SO_2 exhibited larger values in winter and this elevated concentrations might have resulted from (i) residential heating, (ii) enhanced power generation by using high sulfur containing coal combustion, (iii) inferior gas-to-particle conversion, (iv) a lower boundary layer height which prevents dilution of sulfur dioxide. Prevailing meteorological conditions (such as rain and temperature) and type of source may lead to lower NH_3 concentrations in winter compared to summer.

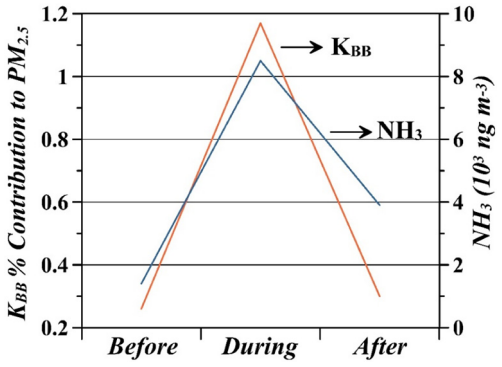

Fig. 10. NH_3 concentrations along with % K_{BB} contributions to $PM_{2.5}$ mass for before (SWS, MED and NW), during (N) and after (N) biomass burning events.

In winter, the diurnal cycle of SO_4^{2-} (11.7 nmol m^{-3}) and SO_2 (42.7 nmol m^{-3}) illustrated their highest concentrations when the airflow originated from the highly populated City of Mersin. Day time increase in NH_3 related positively with temperature and negatively with humidity in winter, suggesting evaporation of dew or emission from plant stoma. HNO_3 peak (at 12.00) followed the NH_4^+ and NO_3^- peaks (at 11.00) and it might be attributed to the dissociation of NH_4NO_3 owing to enhanced temperature and reduced relative humidity. In summer, SO_4^{2-} and NH_4^+ exhibited a broad peak (from 09.00 to 18.00) because of enhanced gas-to-particle conversion. The diurnal cycle of HNO_3 was similar to that of observed for SO_2 ($r = 0.74$, $p < 0.01$), implying a common source for these precursor gases. The diurnal cycle of NH_3 was remarkably altered by emissions from biomass burning in summer.

There was no statistically significant difference between air masses in winter, exhibiting the importance of local or nearly mesoscale transport rather than long range transport. In summer, airflow from Eastern Mediterranean denoted aged air masses containing rather uniform concentrations of SO_4^{2-} (~65 nmol m^{-3}) and NH_4^+ (~140 nmol m^{-3}) as well as gas-to-particle conversion ratios (0.88 and 0.68, respectively). The highest NH_3 concentration was associated with Northerly airflow when the % K_{BB} contribution to $PM_{2.5}$ mass was the largest (1.18%), suggesting the importance of biomass burning emissions as a source of NH_3 in this air mass.

Here we have only presented a relatively short time series (total of 434 h) of near real time measurements of SO_4^{2-}, NH_4^+, NO_3^- (in $PM_{2.5}$), SO_2, NH_3 and HNO_3. There is a clear need to extend temporal and seasonal resolution of such simultaneous measurements including Na^+, K^+, Mg^{2+}, Ca^{2+}, Cl^-, NO_2^-, NO_3^-) in $PM_{2.5}$ and precursor gases (HCl, HONO) as well as NO_x, CO, O_3, black carbon, optical and microphysical properties of aerosols over the Eastern Mediterranean for better comprehension of the atmospheric chemistry and physics of the aerosols. Furthermore, the calculation of the composition and phase state of water-soluble SO_4^{2-}, NH_4^+, NO_3^-, Na^+, K^+, Mg^{2+}, Ca^{2+} and Cl^- in

thermodynamic equilibrium with precursor gases would be useful to understand partitioning of semi-volatile inorganic species.

Acknowledgments

This study was supported by TUBİTAK project (113Y107) and the DEKOSIM (Center for Marine Ecosystem and Climate Research) Project (BAP-08-11-DPT.2012 K120880) funded by Ministry of Development of Turkey. MERRA-2 and MODIS products used in this study were produced with the Giovanni online data system, developed and maintained by the NASA GES DISC.

Appendix A. Supplementary data

Supplementary data to this article can be found online at https://doi.org/10.1016/j.scitotenv.2019.03.451.

References

Appel, B.R., Tokiwa, Y., 1981. Atmospheric particulate nitrate sampling errors due to reactions with particulate and gaseous strong acids. Atmos. Environ. 15 (6), 1087–1089.
Appel, R., Tokiwa, Y., Haik, M., 1980. Sampling of nitrates in ambient air. Atmos. Environ. 15, 283–289.
Appel, B.R., Tokiwa, Y., Haik, M., Kothny, E.L., 1984. Artifact particulate sulfate and nitrate formation on filter media. Atmos. Environ. 18, 409.
Arimoto, R., 2001. Eolian dust and climate: relationships to sources, tropospheric chemistry, transport and deposition. Earth-Sci. Rev. 54, 29–42.
Bardouki, H., Liakakou, H., Economou, C., Sciare, J., Smolik, J., Zdimal, V., Eleftheriadis, K., Lazaridis, M., Dye, C., Mihalopoulos, N., 2003. Chemical composition of size resolved atmospheric aerosols in the eastern Mediterranean during summer and winter. Atmos. Environ. 37, 195–208.
Behera, S.N., Betha, S., Balasubramanian, R., 2013. Insights into chemical coupling among acidic gases, ammonia and secondary inorganic aerosols. Aerosol Air Qual. Res. 13, 1282–1296.
Bennett, D., 1972. A study of the thermal decomposition of ammonium nitrate using a gas chromatographic technique. J. Appl. Chem. 22, 973–982. https://doi.org/10.1002/jctb.5020220904.
Brown, S.S., Ryerson, T.B., Wollny, A.G., Brock, C.A., Peltier, R., Sullivan, A.P., Weber, R.J., Dube, W.P., Trainer, M., Meagher, J.F., Fehsenfeld, F.C., Ravishankara, A.R., 2006. Variability in nocturnal nitrogen oxide processing and its role in regional air quality. Science 311, 67–70.
Chang, Y.S., Carmichael, G.R., Kurita, H., Ueda, H., 1986. An investigation of the formation of ambient NH_4NO_3. Atmos. Environ. 20, 1969–1977.
Cheng, Y., Duan, F.K., He, K.B., Du, Z.Y., Zheng, M., Ma, Y.L., 2012. Intercomparison of thermal-optical method with different temperature protocols: implications from source samples and solvent extraction. Atmos. Environ. 61, 453–462.
Chow, J.C., Doraiswamy, P., Waston, J.G., Chen, L.A., Ho, S.S.H., Sodeman, D.A., 2008. Advances in integrated and continuous measurements for particle mass and chemical composition. J. Air Waste Manage. Assoc. 58, 141–163.
Crutzen, P.J., Andreae, M.O., 1990. Biomass burning in the tropics: impact on atmospheric chemistry and biogeochemical cycles. Science 250, 1669–1678.
Danalatos, D., Glavas, S., 1999. Gas phase nitric acid, ammonia and related particulate matter at a Mediterranean coastal site, Patras, Greece. Atmos. Environ. 33 (20), 3417–3425.
Di Gilio, A., de gennaro, G., Dambruoso, P., Ventrella, G., 2015. An integrated approach using high time-resolved tools to study the origin of aerosols. Sci. Total Environ. 530–531C, 28–37. https://doi.org/10.1016/j.scitotenv.2015.04.073.
Draxler, R.R., 1999. HYSPLIT4 User's Guide. NOAA Tech. Memo. ERL ARL-230, NOAA Air Resources Laboratory, Silver Spring, MD.
Drewnick, F., Schwab, J.J., Hogrefe, O., Peters, S., Husain, L., Diamond, D., Weber, R., Demerjian, K.L., 2003. Intercomparison and evaluation of four semi-continuous $PM_{2.5}$ sulfate instruments. Atmos. Environ. 37, 3335–3350.
Du, H.H., Kong, L.D., Cheng, T., Chen, J., Yang, X., Zhang, R., Han, Z., Yan, Z., Ma, Y., 2010. Insights into ammonium particle-to-gas conversion: non-sulfate ammonium coupling with nitrate and chloride. Aerosol Air Qual. Res. 10, 589–595.
Du, H.H., Kong, L.D., Cheng, T.T., Chen, J.M., Du, J.F., Li, L., Xia, X.G., Leng, C.P., Huang, G.H., 2011. Insights into summertime haze pollution events over Shanghai based on online water-soluble ionic composition of aerosols. Atmos. Environ. 45, 5131e5137.
Ellis, R.A., Murphy, J.G., Markovic, M.Z., VandenBoer, T.C., Makar, P.A., Brook, J., Mihele, C., 2011. The influence of gas-particle partitioning and surface-atmosphere exchange on ammonia during BAQS-Met. Atmos. Chem. Phys. 11, 133–145. https://doi.org/10.5194/acp-11-133-2011.
Gao, X., Yang, L., Cheng, S., Gao, R., Zhou, Y., Xue, L., Shou, Y., Wang, J., Wang, X., Nie, W., Pengju, X., Wang, W., 2011. Semi-continuous measurement of water-soluble ions in $PM_{2.5}$ in Jinan, China: temporal variations and source apportionments. Atmos. Environ. 45, 6048–6056.
Gao, J., Peng, X., Chen, G., Xu, J., Shi, G., Zhang, Y., Feng, Y., 2016. Insights into the chemical characterization and sources of $PM_{2.5}$ in Beijing at a 1-h time resolution. Sci. Total Environ. 542, 162–171. https://doi.org/10.1016/j.scitotenv.2015.10.082.
Godri, K.J., Evans, G.J., Slowik, J., Knox, A., Abbatt, J., Brook, J., Dann, T., Dabek-Zlotorzynska, E., 2009. Evaluation and application of a semi-continuous chemical characterization system for water soluble inorganic $PM_{2.5}$ and associated precursor gases. Atmos. Meas. Tech. 2, 65–80. https://doi.org/10.5194/amt-2-65-2009.
Hauck, H., Berner, A., Frischer, T., Gomiscek, B., Kundi, M., Neuberger, M., Puxbaum, H., Preining, O., AUPHEP Team, 2004. AUPHEP—Austrian project on health effects of particulates—general overview. Atmos. Environ. 38, 3905–3915.
Haywood, J.M., Shine, K.P., 1997. Multi-spectral calculations of the radiative forcing of tropospheric sulphate and soot aerosols using a column model. Q. J. R. Meteorol. Soc. 123, 1907–1930.
Hegg, D.A., Radke, L.F., Hobbs, P.V., Riggan, P.J., 1988. Ammonia emissions from biomass burning. Geophys. Res. Lett. 15 (4), 335–337.
Hering, S., Cass, G., 1999. The magnitude of bias in the measurement of $PM_{2.5}$ arising from volatilization of particulate nitrate from Teflon filters. J. Air Waste Manage. Assoc. 49 (6), 725–733. https://doi.org/10.1080/10473289.1999.10463843.
Hu, G., Zhang, Y., Sun, J., Zhang, L., Shen, X., Lin, W., Yang, Y., 2014. Variability, formation and acidity of water-soluble ions in $PM_{2.5}$ in Beijing based on the semi-continuous observations. Atmos. Res. 145–146, 1–11. https://doi.org/10.1016/j.atmosres.2014.03.014.
Huang, J., Lin, B., Minnis, P., Wang, T., Wang, X., Hu, Y., Yi, Y., Ayers, J.K., 2006. Satellite-based assessment of possible dust aerosols semidirect effect on cloud water path over East Asia. Geophys. Res. Lett. 33, L19802. https://doi.org/10.1029/2006GL026561.
Jickells, T.D., An, Z.S., Andersen, K.K., Baker, A.R., Bergametti, G., et al., 2005. Global iron connections between desert dust, ocean biogeochemistry and climate. Science 308, 67–71.
Jordi, A., Basterretxea, G., Tovar-Sánchez, A., Alastuey, A., Querol, X., 2012. Copper aerosols inhibit phytoplankton growth in the Mediterranean Sea. Proc. Natl. Acad. Sci. U. S. A. 109, 21246–21249.
Kadowaki, S., 1986. On the nature of atmospheric oxidation processes of SO_2 to sulfate and of NO_2 to nitrate on the basis of diurnal variations of sulfate, nitrate, and other pollutants in an urban area. Environ. Sci. Technol. 20, 1249–1253.
Keck, L., Wittmaack, K., 2005. Effect of filter type and temperature on volatilisation losses from ammonium salts in aerosol matter. Atmos. Environ. 39, 4093–4100. https://doi.org/10.1016/j.atmosenv.2005.03.029.
Khoder, M.I., 2002. Atmospheric conversion of sulfur dioxide to particulate sulfate and nitrogen dioxide to particulate nitrate and gaseous nitric acid in an urban area. Chemosphere 49, 675–684.
Koçak, M., Mihalopoulos, N., Kubilay, N., 2007. Chemical composition of the fine and coarse fraction of aerosols in the northeastern Mediterranean. Atmos. Environ. 41, 7351–7368.
Koçak, M., Mihalopoulos, N., Kubilay, N., 2009. Origin and source regions of PM_{10} in the eastern Mediterranean atmosphere. Atmos. Res. 92, 464–474.
Koçak, M., Theodosi, C., Zarmpas, P., Im, U., Bougiatioti, A., Yenigun, O., Mihalopoulos, N., 2011. Particulate matter (PM_{10}) in Istanbul: origin, source areas and potential impact on surrounding regions. Atmos. Environ. 45, 6891–6900.
Koçak, M., Theodosi, C., Zarmpas, P., Séguret, M.J.M., Herut, B., Kallos, G., Mihalopoulos, N., Kubilay, N., Nimmo, M., 2012. Influence of mineral dust transport on the chemical composition and physical properties of the Eastern Mediterranean aerosol. Atmos. Environ. 57, 266–277.
Koçak, M., Mihalopoulos, N., Tutsak, E., Violaki, K., Theodosi, C., Zarmpas, P., Kalegeri, P., 2016. Atmospheric Deposition of Macro Nutrients (DIN and DIP) onto the Black Sea and implications on marine productivity. J. Atmos. Sci. 13, 1727–1739. https://doi.org/10.1175/JAS-D-15-0039.1.
Kouvarakis, G., Mihalopoulos, N., Tselepides, T., Stavrakakis, S., 2001. On the importance of atmospheric nitrogen inputs on the productivity of Eastern Mediterranean. Glob. Biogeochem. Cycles 15, 805–818.
Kouvarakis, G., Bardouki, H., Mihalopoulos, N., 2002. Sulfur budget above the Eastern Mediterranean: relative contribution of anthropogenic and biogenic sources. Tellus Ser. B Chem. Phys. Meteorol. 54 (3), 201–212. https://doi.org/10.3402/tellusb.v54i3.16661.
Krueger, B.J., Grassian, V.H., Cowin, J.P., Laskin, A., 2004. Heterogeneous chemistry of individual mineral dust particles from different dust source regions: the importance of particle mineralogy. Atmos. Environ. 38, 6253–6261.
Kubilay, N., Saydam, C., 1995. Trace elements in atmospheric particulates over the Eastern Mediterranean: concentration, sources and temporal variability. Atmos. Environ. 29, 2289–2300.
Lee, S., Liu, W., Wang, Y.H., Russell, A.G., Edgerton, E.S., 2008. Source apportionment of $PM_{2.5}$: comparing PMF and CMB results for four ambient monitoring sites in the southeastern United States. Atmos. Environ. 42 (18), 4126–4137.
Lelieveld, J., Berresheim, H., Borrmann, S., Crutzen, P.J., Dentener, F.J., Fischer, H., Feichter, J., Flatau, P., Heland, J., Holzinger, R., Kormann, R., Lawrence, M.B., Levin, Z., Markowicz, K., Mihalopoulos, N., Minikin, A., Ramanthan, V., de Reus, M., Roelofs, G.J., Scheeren, H.A., Sciare, J., Schlager, H., Schulz, M., Siegmund, P., Steil, B., Stephanou, E.G., Stier, P., Traub, M., Warneke, C., Williams, J., Ziereis, H., 2002. Global air pollution crossroads over the Mediterranean. Science 298, 794–799.
Levin, Z., Teller, A., Ganor, E., Yin, Y., 2005. On the interactions of mineral dust, sea salt particles and clouds – measurements and modeling study from the MEIDEX campaign. J. Geophys. Res. 110, D20202. https://doi.org/10.1029/2005JD005810.
Lipfert, F., 1994. Filter artifacts associated with particulate measurements: recent evidence and effects on statistical relationships. Atmos. Environ. 28, 3233–3249. https://doi.org/10.1016/1352-2310(94)00167-J.
Liu, W., Wang, Y.H., Russell, A., Edgerton, E.S., 2005. Atmospheric aerosol over two urban-rural pairs in the southeastern United States: chemical composition and possible sources. Atmos. Environ. 39 (25), 4453–4470.
Luria, M., Peleg, M., Sharf, G., Tov-Alper, D.S., Spitz, N., Ben Ami, Y., Gawii, Z., Lifschitz, B., Yitzchaki, A., Seter, I., 1996. Atmospheric sulfur over the east Mediterranean region. J. Geophys. Res. 101, 25917–25930.

Ma, Y., Weber, R.J., Lee, Y.-N., Orsini, D.A., Maxwell-Meier, K., Thornton, D.C., Bandy, A.R., Clarke, A.D., Blake, D.R., Sachse, G.W., Fuelberg, H.E., Kiley, C.M., Woo, J.-H., Streets, D.G., Carmichael, G.R., 2003. Characteristics and influence of biosmoke on the fine-particle ionic composition measured in Asian outflow during the Transport and Chemical Evolution Over the Pacific (TRACE-P) experiment. J. Geophys. Res. 108 (D21), 8816. https://doi.org/10.1029/2002JD003128.

Mahowald, N.M., Baker, A.R., Bergametti, G., Brooks, N., Duce, R.A., et al., 2005. Atmospheric global dust cycle and iron inputs to the ocean. Glob. Biogeochem. Cycles 19, GB4025. https://doi.org/10.1029/2004GB002402.

Makkonen, U., Virkkula, A., Mäntykenttä, J., Hakola, H., Keronen, P., Vakkari, V., Aalto, P.P., 2012. Semi-continuous gas and inorganic aerosol measurements at a Finnish urban site: comparisons with filters, nitrogen in aerosol gas phases, and aerosol acidity. Atmos. Chem. Phys. 12, 5617–5631.

Makkonen, U., Virkkula, A., Hellén, H., Hemmilä, M., Sund, J., Hakola, H., Äijälä, M., Ehn, M., Junninen, H., Keronen, P., Petäjä, T., Worsnop, R.D., Kulmala, M., 2014. Semi-continuous gas and inorganic aerosol measurements at a boreal forest site: seasonal and diurnal cycles of NH_3, HONO and HNO_3. Boreal Environ. Res. 19, 311–328.

Malaguti, A., Mircea, M., La Torretta, M.G.T., Telloli, C., Petralia, E., Stracquadanio, M., Berico, M., 2015. Comparison of online and offline methods for measuring fine secondary inorganic ions and carbonaceous aerosols in the Central Mediterranean area. Aerosol Air Qual. Res. 15, 2641–2653. https://doi.org/10.4209/aaqr.2015.04.0240.

Markovic, M.Z., VandenBoer, T.C., Murphy, J.G., 2012. Characterization and optimization of an online system for the simultaneous measurement of atmospheric water-soluble constituents in the gas and particle phases. J. Environ. Monit. 14, 1872–1884. https://doi.org/10.1039/C2EM00004K.

Markovic, M.Z., VandenBoer, T.C., Baker, K.R., Kelly, J.T., Murphy, J.G., 2014. Measurements and modeling of the inorganic chemical composition of fine particulate matter and associated precursor gases in California's San Joaquin Valley during CalNex 2010. J. Geophys. Res. Atmos. 119, 6853–6866. https://doi.org/10.1002/2013JD021408.

Millero, F.J., Sohn, M.L., 1992. Chemical Oceanography. CRC Press, Boca Raton, Fla (531 pp.).

Nie, W., Wang, T., Gao, X., Pathak, R.K., Wang, X., Gao, R., Zhang, Q., Yang, L., Wang, W.X., 2010. Comparison among filter-based, impactor-based and continuous techniques for measuring atmospheric fine sulfate and nitrate. Atmos. Environ. 44, 4396–4403. https://doi.org/10.1016/j.atmosenv.2010.07.047.

Pakkanen, T.A., Hillamo, R.E., Aurela, M., Andersen, H.V., Grundahl, L., Ferm, M., Persson, K., Karlsson, V., Reissell, A., Royset, O., Floisand, I., Oyola, P., Ganko, T., 1999. Nordic intercomparison for measurement of major atmospheric nitrogen species. J. Aerosol Sci. 30, 247–263.

Paytan, A., Mackey, K.R.M., Chen, Y., Limac, I.D., Doneyc, S.C., Mahowaldd, N., Labiosae, R., Postf, A.F., 2009. Toxicity of atmospheric aerosols on marine phytoplankton. Proc. Natl. Acad. Sci. U. S. A. https://doi.org/10.1073/pnas.08114868106.

Pio, C.A., Legrand, M., Alves, C.A., Oliveira, T., Afonso, J., Caseiro, A., Puxbaum, H., Sanchez-Ochoa, A., Gelencser, A., 2008. Chemical composition of atmospheric aerosols during the 2003 summer intense forest fire period. Atmos. Environ. 42, 7530–7543.

Ramadan, Z., Song, X.H., Hopke, P.K., 2000. Identification of sources of Phoenix aerosol by positive matrix factorization. J. Air Waste Manage. Assoc. 50 (8), 1308–1320.

Roelle, A.P., Aneja, V., 2002. Characterization of ammonia emissions from soils in the upper coastal plain, North Carolina. Atmos. Environ. 36, 1087–1097. https://doi.org/10.1016/S1352-2310(01)00355-7.

Rosenfeld, D., Lohmann, U., Raga, G.B., O'Dowd, C.D., Kulmala, M., Fuzzi, S., Reissell, A., Andreae, M.O., 2008. Flood or drought: how do aerosols affect precipitation? Science 321, 1309–1313.

Salma, I., Balashazy, I., Winkler-Heil, R., Hofmann, W., Zaray, G., 2002. Effect of particle mass size distribution on the deposition of aerosols in the human respiratory system. Aerosol Sci. 33, 119–132.

Savoie, D.L., Prospero, J.M., Oltmans, S.J., Graustein, W.C., Turekian, K.K., Merrill, J.T., Levy, H., 1992. Sources of nitrate and ozone in the marine boundary layer of the tropical north Atlantic. J. Geophys. Res. 97 (D11), 11575–11589.

Schaap, M., Mueller, K., ten Brink, H.M., 2002. Constructing the European aerosol nitrate concentration field from quality analysed data. Atmos. Environ. 36, 1323–1335.

Schaap, M., Spindler, G., Schulz, M., Acker, K., Maenhaut, W., Berner, A., Wieprecht, W., Streit, N., Muller, K., Bruggemann, E., Chi, X., Putaud, J.P., Hitzenberger, R., Puxbaum, H., Baltensperger, U., ten Brink, H., 2004. Artefacts in the sampling of nitrate studied in the "INTERCOMP" campaigns of EUROTRAC-AEROSOL. Atmos. Environ. 38, 6487–6496.

Seinfeld, J.H., Pandis, S.N., 1998. Atmospheric Chemistry and Physics: From Air Pollution to Climate Change. J. Wiley, New York.

Shi, Y., Chen, J., Hu, D., Wang, L., Yang, X., Wang, X., 2014. Airborne submicron particulate (PM_1) pollution in Shanghai, China: chemical variability, formation/dissociation of associated semivolatile components and the impacts on visibility. Sci. Total Environ. 473, 199–206.

Shon, Z.H., Kim, K.H., Song, S.K., Jung, K., Kim, N.J., Lee, J.B., 2012. Relationship between water-soluble ions in $PM_{2.5}$ and their precursor gases in Seoul megacity. Atmos. Environ. 59, 540–550. https://doi.org/10.1016/j.atmosenv.2012.04.033.

Shon, Z.H., Ghosh, S., Kim, K.H., Song, S.K., Jung, K., Kim, N.J., 2013. Analysis of water-soluble ions and their precursor gases over diurnal cycle. Atmos. Res. 132, 309–321.

Stein, A.F., Draxler, R.R., Rolph, G.D., Stunder, B.J.B., Cohen, M.D., Ngan, F., 2015. NOAA's HYSPLIT atmospheric transport and dispersion modeling system. Bull. Am. Meteorol. Soc. 96, 2059–2077. https://doi.org/10.1175/BAMS-D-14-00110.1.

Ten Brink, H.M., Otjes, R.P., Jongejan, P., Slanina, S., 2007. An instrument for semi-continuous monitoring of the size-distribution of nitrate, ammonium, sulphate and chloride in aerosol. Atmos. Environ. 41, 2768–2779, 2007.

Tian, M., Wang, H.B., Chen, Y., Zhang, L.M., Shi, G.M., Liu, Y., Yu, J.Y., Zhai, C.Z., Wang, J., Yang, F.M., 2017. Highly time-resolved characterization of water-soluble inorganic ions in $PM_{2.5}$ in a humid and acidic mega city in Sichuan Basin, China. Sci. Total Environ. 580, 224–234. https://doi.org/10.1016/j.scitotenv.2016.12.048.

Tsai, C., Perng, S., 1998. Artifacts of ionic species for hi-vol PM_{10} and PM_{10} dichotomous samplers. Atmos. Environ. 32, 1605–1613. https://doi.org/10.1016/S1352-2310(97)00387-7.

Ullah, S., Takeuchi, M., Dasgupta, P., 2006. Versatile gas/particle ion chromatograph. Environ. Sci. Technol. 40, 962–968. https://doi.org/10.1021/es051722z.

Usher, C.R., Michel, A.E., Grassin, V.H., 2003. Reactions on mineral dust. Chem. Rev. 103, 4883–4939.

Vecchi, R., Valli, G., Fermo, P., D'Alessandro, A., Piazzalunga, A., Bernardoni, V., 2009. Organic and inorganic sampling artefacts assessment. Atmos. Environ. 43, 1713–1720. https://doi.org/10.1016/j.atmosenv.2008.12.016.

Weber, R.J., Orsini, D., Daun, Y., Lee, Y.N., Klotz, P.J., Brechtel, F.J., 2001. A particle-into-liquid collector for rapid measurement of aerosol bulk chemical composition. Aerosol Sci. Technol. 35, 718–727.

Wentworth, G.R., Murphy, J.G., Gregoire, P.K., Cheyne, C.A.L., Tevlin, A.G., Hems, R., 2014. Soil–atmosphere exchange of ammonia in a non-fertilized grassland: measured emission potentials and inferred fluxes. Biogeosciences 11, 5675–5686. https://doi.org/10.5194/bg-11-5675-2014.

Wentworth, G.R., Murphy, J.G., Benedict, K.B., Bangs, E.J., Collett Jr., J.L., 2016. The role of dew as a night-time reservoir and morning source for atmospheric ammonia. Atmos. Chem. Phys. 16, 7435–7449. https://doi.org/10.5194/acp-16-7435-2016.

Wieprecht, W., Acker, K., Müller, K., Spindler, G., Brüggemann, E., Maenhaut, W., Chi, X., Hitzenberger, R., Bauer, H., ten Brink, H., 2004. INTERCOMP2000: ionic constitution and comparison of filter and impactor. Atmos. Environ. 38, 6477–6486.

Wittig, A.E., Pandis, S.N., Hering, S., Kirby, B., Khlystov, A.Y., Takahama, S., Davidson, C.I., 2004. Semicontinuous $PM_{2.5}$ inorganic composition measurements during the Pittsburgh Air Quality Study. Atmos. Environ. 38, 3201–3213.

Xue, J., Lau, A.K., Yu, J.Z., 2011. A study of acidity on $PM_{2.5}$ in Hong Kong using online ionic chemical composition measurements. Atmos. Environ. 45 (39), 7081–7088.